

# Characterization and Manufacture of Braided Composites for Large Commercial Aircraft Structures<sup>1</sup>

Mark J. Fedro  
Boeing Defense and Space Group - Philadelphia, PA

Kurtis Willden  
Boeing Commercial Airplane Group - Seattle, WA

NASA  
516-24  
51356  
P-44  
200

## ABSTRACT

Braided composite materials, one of the advanced material forms which is under investigation in Boeing's ATCAS program, have been recognized as a potential cost-effective material form for fuselage structural elements. Consequently, there is a strong need for more knowledge in the design, manufacture, test, and analysis of textile structural composites. The overall objective of this work is to advance braided composite technology towards applications to a large commercial transport fuselage. This paper summarizes the mechanics of materials and manufacturing demonstration results which have been obtained in order to acquire an understanding of how braided composites can be applied to a commercial fuselage. Textile composites consisting of 2-D, 2-D triaxial, and 3-D braid patterns with thermoplastic and two RTM resin systems were investigated. The structural performance of braided composites was evaluated through an extensive mechanical test program. Analytical methods were also developed and applied to predict the following: internal fiber architectures, stiffnesses, fiber stresses, failure mechanisms, notch effects, and the entire history of failure of the braided composite specimens. The applicability of braided composites to a commercial transport fuselage was further assessed through a manufacturing demonstration. Three foot fuselage circumferential hoop frames were manufactured to demonstrate the feasibility of consistently producing high quality braided/RTM composite primary structures. The manufacturing issues (tooling requirements, processing requirements, and process/quality control) addressed during the demonstration are summarized. The manufacturing demonstration in conjunction with the mechanical test results and developed analytical methods increased the confidence in the ATCAS approach to the design, manufacture, test, and analysis of braided composites.

## INTRODUCTION

Textile structural composites represent a class of advanced materials in which a light-weight matrix material is reinforced with a textile fiber preform. The potential for significant cost savings for textile reinforced composites through automated preform fabrication and low-cost resin transfer molding (RTM) has increased the commercial airplane industry interest in these materials. As the use of composites is being expanded to large scale structural components, textile reinforcements are being considered for providing adequate structural integrity as well as process flexibility for near-net-shape manufacturing.

Boeing's program for Advanced Technology Composite Aircraft Structures (ATCAS) has focused on the manufacturing and performance issues associated with a wide body commercial transport fuselage. The main ATCAS objective is to develop an integrated technology and demonstrate a confidence level that permits cost- and weight-effective use of advanced composite materials in future primary aircraft structures with the emphasis on pressurized fuselages. An aft fuselage section directly behind the wing-to-body intersection is used for technology development and verification purposes in ATCAS. This section of fuselage (shown in Figure 1) has many design details and associated technology issues that pose a test of advancements in composite primary structures.

<sup>1</sup> This work was funded by Contract NAS1-18889, under the direction of J.G. Davis and W.T. Freeman of NASA Langley Research Center.

The ATCAS Program uses a Design Build Team (DBT) Approach and a 3-step design process. The first step in the design process is the selection of Baseline Concepts as those design and manufacturing ideas having an apparent potential for cost and weight savings, combined with an acceptable risk; technology issues are also identified during this phase of design. The second step is Global Evaluation where cost and weight savings are evaluated by performing detailed studies for the baseline and a limited number of alternative concepts. The final step in the design process is Local Optimization in which cost centers and major technology barriers established during the first two design steps are attacked. The design families chosen during the design process are shown in Figure 2.

During the ATCAS design process, the DBT recognized that textile composites have a great potential for many applications to primary structural components in a fuselage. The potential structural applications of textile composites (shown in Figure 2) are the circumferential hoop frames, the window belt, and the underfloor cargo frames.

The crown panel section was the first quadrant of focus in the ATCAS Program. The ATCAS DBT performed several comparative studies of different potential textile material systems for the circumferential hoop frames. Using the results of the comparative studies, 2-D triaxially braided/RTM material systems exhibited the most promise. The focus of this paper is the characterization and manufacture of braided composites for the crown panel frames. A detailed outline of this paper is shown in Figure 3. The first section of this paper describes the global selection and requirements of the crown panel circumferential hoop frames. Section 2 details the braided/RTM technology development in the areas of materials, manufacturing, analysis, and test. Section 3 describes the details of the 3 ft. frame manufacturing demonstration and the technology that supported the demonstration. Section 4 gives the details on the Local Optimization of the frame design. Finally, the scale-up issues for a half-length manufacturing demonstration are identified and discussed in the final section of the paper.

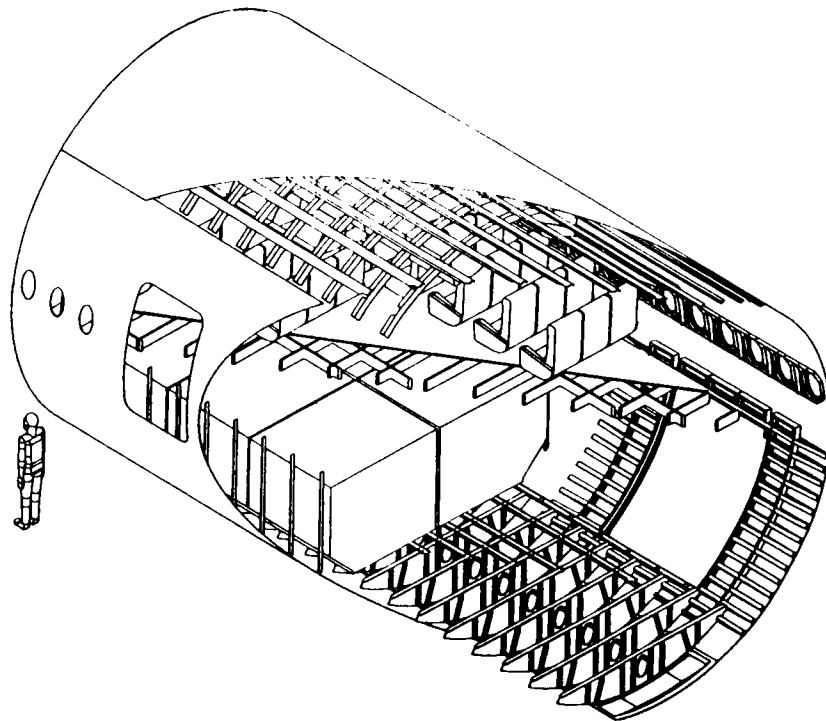


**Figure 1: ATCAS Fuselage Design**

## CROWN PANEL

## SIDE PANEL

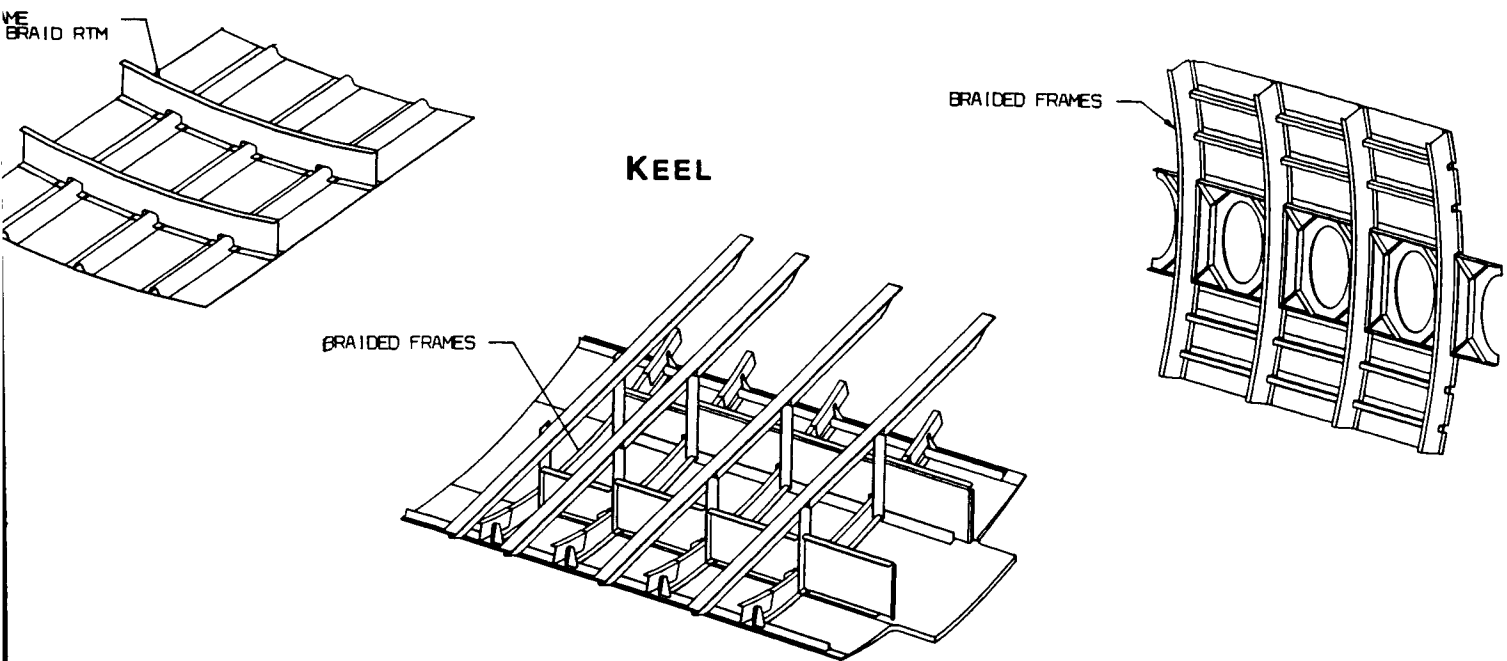


**Figure 2: Potential Fuselage Applications for Textile Composites**

### 1. GLOBAL SELECTION AND REQUIREMENTS

- A. Material and Manufacturing Cost Evaluation
- B. Design Requirements
- C. Manufacturing Requirements

### 2. BRAIDED/RTM TECHNOLOGY DEVELOPMENT

- A. Braided Composite Material Systems
- B. Manufacturing of Braided Composites
- C. ATCAS Textile Composites Analysis (TECA)
- D. Mechanical Characterization of Braided Composites

### 3. CIRCUMFERENTIAL HOOP FRAME DEVELOPMENT

- A. Material Selection
- B. Frame Fiber Architecture Design
- C. Manufacturing of Braided Composite Specimens
- D. Material System Performance Evaluation
- E. 3 ft Frame Manufacturing Demonstration

### 4. FRAME DESIGN LOCAL OPTIMIZATION

- A. Dimensional Accuracy Optimization
- B. Frame-to-Skin Bond Issue
- C. Mouse Hole Configuration
- D. Manufacturing Process Optimization
- E. Cost and Weight Impact of Local Design Optimization
- F. Summary of Current Circumferential Hoop Frame Design

### FUTURE WORK / KEY ACCOMPLISHMENTS

### Figure 3: Paper Outline

# 1. FRAME GLOBAL SELECTION AND REQUIREMENTS

## A. Material and Manufacturing Cost Evaluation

Four different material systems and fabrication techniques were screened as possible candidates for the circumferential hoop frames during the detailed cost and weight studies. The four material systems and the fabrication techniques were: 1) stretch forming long discontinuous fibers (LDF), 2) compression molding fabric prepreg, 3) pultruding dry fiber through a resin bath, and 4) RTM 2-D braided preforms. A price per pound comparison of frame fabrication processes and material systems is found in Reference 1. Results of this study show that the 2-D braided/RTM material system was the most attractive process in terms of cost, weight, and manufacturability for the circumferential hoop frames; the cost of the braided RTM frames was approximately \$85/lb. This material system and fabrication technique uses the constituent materials in their lowest cost form. Braiding is a continuous, high-rate automated preform process that provides net-shape manufacturing which minimizes machining and trimming and produces preform dimensional accuracy. The fiber architecture of the preforms can also be tailored to meet design criteria. RTM provides batch-mode capabilities and repeatable closed-mold tolerances. Braided/RTM material systems tend to be more dimensionally stable than other systems such as tape, in addition the flexibility inherent to both braiding and RTM is advantageous in fabricating large complex structural composite components.

The skin/stringer/frame design was based on the use of automated systems that were considered highly efficient. Computer automated advanced tow placement was selected to lay-up the skins. A contoured tape lamination machine (CTLM), followed by a drape forming process was selected to lay-up and shape the hat stiffeners. Finally, the autoclave fabrication of full crown quadrant segments is envisioned as wet skin and stiffener, co-bonded with frames [2].

## B. Design Requirements

Fuselage frames serve a number of different functions. They maintain the cross sectional shape of the fuselage, resist the pressure-induced hoop loads (in conjunction with the skin), distribute concentrated loads, redistribute shear loads around structural discontinuities, and limit the column length of the longitudinal stringers to prevent general instability. The frames with flanges attached to the fuselage skin also act in a fail safe capacity as circumferential tear straps to restrict damage propagation.

### 1.B.1 Frame Configuration

The current configuration of the frame is a J-section with its wide flange (or cap) co-bonded to automated tow-placed skin. An I-section was considered for the frames, but was dismissed due to the difficulty of allowing attachments. A Z-section is undesirable for bonded structure due to peel stresses which develop with loads normal to the skin. A J-section, however, can easily accommodate attachment details and is not as prone to peel stresses because its web is located symmetrical with respect to the bonded flange. A limit for the total depth of the frame, including the attached skin, was assumed at 5.5 inches to maximize the useful space inside the fuselage. The J frames are mouse holed to accommodate the stringers. The frame configuration selected during global evaluation is shown in Figure 4.

The bending stiffness of the frame cap must be less than than the bending stiffness of the skin to prevent excessive peel stresses from occurring during pressure pillowing of the skin. Since the frame-to-skin intersection is designed for failure to occur at the bond line, the cap must be designed to resist internal crack initiation. The frame configuration selected during global evaluation contains 3 layers of braided fabric on the frame cap to aid in manufacturing. The filler pack shown in Figure 4 must be added to the cap of the frame to fill the void caused by the splitting and separation of braided layers during frame fabrication. The filler pack material must be tough enough to resist crack initiation and propagation during frame loading.

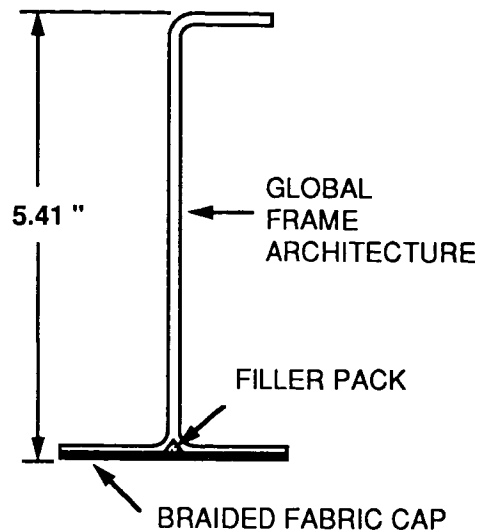


**Figure 4: Frame Configuration Selected During Global Evaluation**

### 1.B.2 Critical Stiffness Design Criteria

The four critical load cases for the fuselage crown panel were determined to be: 1) ultimate internal pressure, 2) 6G up gust, 3) 9G forward crash condition, and 4) 3G down gust. Of these four cases, the ultimate pressure loading condition is the most critical condition for the circumferential hoop frames located in the crown panel. The ultimate pressure of 18.2 psi represents two times the normal operating pressure and corresponds to hoop direction line load of 2220 lb/in for a fuselage with a 122 inch radius. The hoop load puts the frame in axial tension, but bending loads also result as the pressure tries to stretch the frame to a larger radius. The frame spacing on the crown panel is typically 22 inches which was determined by stiffener stability, crown panel weight, and fuselage geometry requirements (ex. doors, window belt, etc.).

The pressure case also produces pull-off loads to balance the axial tension in the curved frames. The magnitude of the pull-off loads is proportional to the percentage of the load in the frame relative to the skin. These loads are critical to the strength and durability issues of the frame-to-skin bond line.

The frame loads are critical at the location of the mouse hole cut-outs where the cross sectional properties are significantly reduced. The critical ultimate pressure condition includes bending loads which produce a maximum strain at the inner flange of the frame. Design strains at ultimate load were limited to 0.5% tension and 0.4% compression for damage tolerance considerations. The effect of stress concentrations at the mouse holes is not a design driver since the edge of the mouse hole cut-out is in the middle of the bending section, away from the highly stressed frame inner flange.

The stiffness of the frames was checked to ensure that general instability of the fuselage does not occur. The criterion establishes a minimum bending stiffness of the frame as follows [3]:

$$(EI)_{\text{frame}} = \frac{MD^2}{16000 L} \quad \text{where: } M = \text{bending moment on fuselage} \quad (1)$$

$$D = \text{diameter of fuselage}$$

$$L = \text{frame spacing}$$

### 1.B.3 Mouse Hole Configuration

The frames incorporate mouse hole cut-outs to allow the continuous stringers through the frame-to-stringer intersections. The size of the cut-outs must be kept as small as possible to minimize the reduction of frame cross-sectional properties and still meet assembly requirements. In the crown section of the fuselage, the mouse holes span the entire width of the hat stringers for ease of assembly.

The column stability of the stringers requires the frames to provide enough stiffness normal to the stiffened skin such that a node point is achieved at each frame-to-stringer intersection. The mouse holes at these locations reduce the stiffness and compromise the ability of the frames to force a node point. Due to this reduction in stiffness, sections of the fuselage which are subjected to high axial compression loads often require a clip which forms a direct attachment between the stringer and the web of the frame at the mouse hole. In the crown, however, the axial compression loads are relatively small and the stringer clips were determined to be unnecessary. This conclusion will be verified later by large scale stability tests. The mouse hole detail selected during global evaluation is shown in Figure 5.

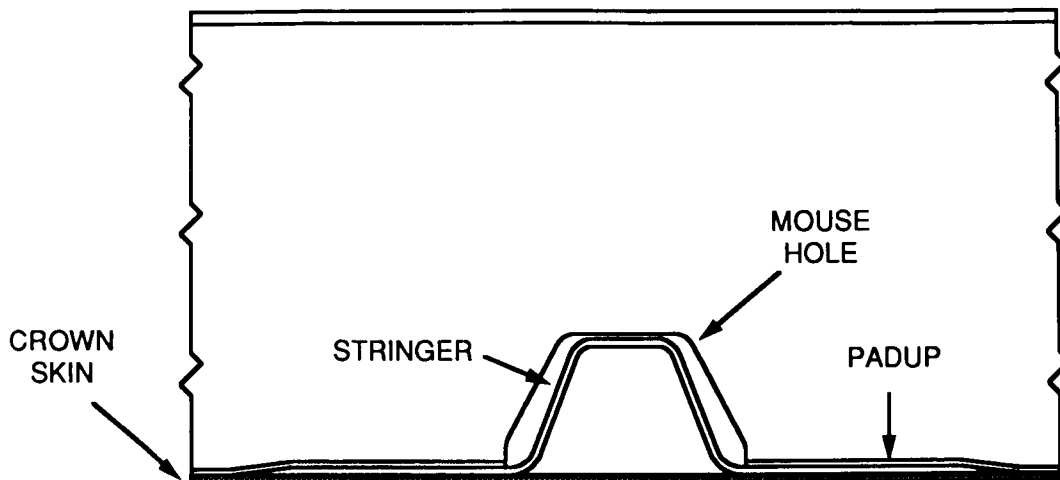


Figure 5: Mouse Hole Configuration Selected During Global Evaluation

### 1.B.4 Frame-to-Skin Bondline

One major technical issue identified for the crown panel design is the strength and durability of adhesively bonded frame elements. The crown frame bond line is subjected to pull-off forces from cabin pressure and post-buckled skins. Real time aspects of the problem needed to be considered since bond line stresses change as a function of cyclic pressure conditions. The strength and durability of adhesive bond lines that attach braided frames to automated tow-placed skins must be studied using both test and analysis.

## C. Manufacturing Requirements

The manufacturing requirements selected for RTM braided frames include: suitable RTM resin system, repeatable high quality part producibility and process control, batch mode manufacturing, and integration of process automation.

### 1.C.1 RTM Resin Requirements

In choosing an RTM resin system for the circumferential hoop frames, the ATCAS DBT screened RTM resin systems using 3 criteria: 1) manufacturability, 2) structural performance, and 3) cost. To manufacture circumferential frames the desired pot life is one hour with a viscosity of less than 50 centipoise (typical injection time is under 15 minutes). Processing anomalies are minimized with a resin system that offers low injection viscosity and a long pot life. Since the RTM frames are co-bonded to the

skin, the resin must be stable for an additional 5 hours at temperature greater than 350°F without property loss, therefore the glass transition temperature of the resin must be above 350°F. The structural performance of the resin must meet the necessary ATCAS stiffness, strength, damage tolerance, and environmental resistance requirements. Finally, the cost of the resin must be reasonable in order for composite design to compete with aluminum design.

### **1.C.2 Producibility and Process Control**

The RTM operation must achieve full wet-out conditions in order to satisfy the ATCAS criteria of less than a 2% void content of a finished composite part. In order to meet this requirement, accurate process control is needed to ensure that the resin is injected at the right viscosity and pressure. A constant resin viscosity must be maintained by accurate temperature control of the mixing pot and the entire RTM tool to avoid premature gelation and exothermal reactions. Feedback control of the temperature is essential and is considered a major parameter for SPC (Statistical Process Control) of part producibility. Optimization and control of injection ports, vacuum ports, and the resin system cure cycle are required to assist in the proper wet-out of the preforms.

### **1.C.3 Batch Mode Requirements**

To increase process efficiency, batch mode processing must be employed to reduce tooling and processing labor costs. Two batch mode processes were considered for the 2-D braided/RTM material system. Both processes use the mandrel containing the braided layers as part of the RTM tooling to minimize handling and inspection. In the first type of batch mode process, several mandrels containing the braided preforms are stacked side-by-side in a mold cavity and then the preforms are cut and folded into the desired frame geometry. In the second batch mode process, the mandrels containing the braided preforms are placed into individual mold cavities followed by the cutting and folding. The second method was chosen because the batch size is adjustable for any production requirement without tooling modifications and dimension stability can be accurately controlled with individual mold cavities. In addition, the second process requires fewer mandrels and the braided preform is more accessible which is advantageous during preform assembly.

### **1.C.4 Process Automation**

To maximize the effectiveness of the RTM and braiding operations, automation concepts must be employed for high production rates. Careful selection must be made to ensure that the selected concepts minimize the sensitivity to frame design changes. One of the main limitations of the braiding operation that needs to be overcome is the machine material capacity. Currently, a 144 carrier braider contains spools that are designed to carry less than 0.3 pound of graphite fiber. A fully loaded braider operating at a high speed (4 ft/min) must be reloaded in approximately two hours. To minimize reloading time, future spool sizes should be designed to store 2-3 pounds of graphite. Another requirement of the automation process is that handling should be kept to a minimum in order to reduce inspection.

### **1.C.5 Dimensional Stability**

Dimensional stability of the circumferential hoop frames is critical because the crown panel design involves the assembly of large stiff fuselage structures. Large panel structures must be spliced together, therefore tight tolerances must be achieved on each structural component to minimize assembly problems. In addition to panel splices, the assembly of the crown panel design involves co-bonding precured structural components to uncured components and dimensional stability is extremely important in this type of operation. In addition to assembly concerns, dimensional stability is required to avoid problems with residual stresses.

As previously mentioned, the dimensional stability and accuracy of the frames are critical to the success of the skin/stringer/frame assembly. Two dimensions that influence the performance of the bond line are the

122 inch radius of the frame and the bottom flange-to-web perpendicularity. The frame bottom flange radius must be accurate to minimize the gap that may occur due to tolerance build-up at the skin/stringer/frame intersection. The tolerances of the flange radius must be controlled by proper tool design and optimization of the RTM processing parameters. The spring-in condition of the flanges must be compensated by the proper tool design.

## **2. BRAIDED/RTM TECHNOLOGY DEVELOPMENT**

The original goals of the Technology Development Phase were: 1) to acquire an understanding of the state-of-the-art in braided composite technology, 2) to conduct a general screening of braided composites, and 3) to identify potential applications (such as shear clips, shear ties, or stringers) for braided composites in a large commercial transport fuselage. Shortly after this Phase started, the ATCAS DBT identified braided composites as a potential cost-effective material system for primary fuselage structures. It was also discovered that braided composite technology had not progressed to the point where braided composites could be designed into an aircraft fuselage. The Technology Development Phase then refocused its overall goal to advance the state-of-the-art in braided composite technology and build a confidence level to support the design efforts of the baseline fuselage concepts containing textile composites. The four main areas of focus of this Phase were refocused to the following: 1) Braided Composite Material Systems, 2) Manufacturing of Braided Composites, 3) Textile Composite Analysis, and 4) Mechanical Characterization of Braided Composites.

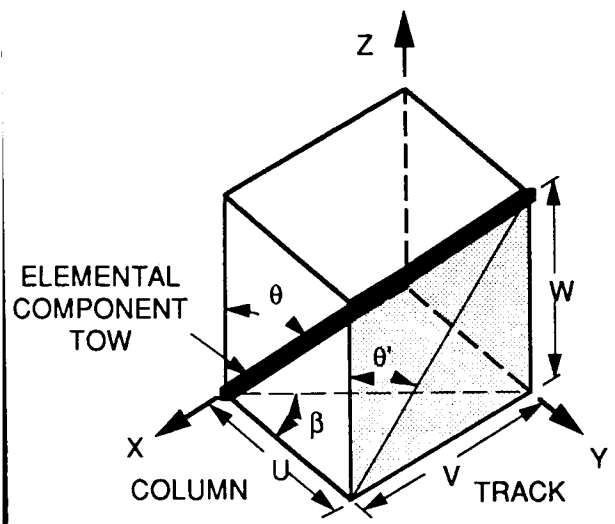
### **A. Braided Composite Material Systems**

#### **2.A.1 Material Selection**

Two material systems were investigated in the Technology Development Phase, a graphite/thermoplastic material system and a graphite/RTM resin material system. The graphite/thermoplastic material system chosen for this study was AS4/PEEK. The preform material used in this system was a commingled AS4/PEEK hybrid yarn; the graphite contained in this yarn was an AS4 3K fiber tow and the grade of PEEK was 150G. The graphite/RTM resin material system chosen was AS4/DPL-862; the preform material used in this system was an AS4 3K fiber tow and the resin system was Shell's DPL-862 and curing agent "W". This resin system was chosen for its cost (\$2.65/lb) and its manufacturability (viscosity profile suitable for RTM).

#### **2.A.2 Fiber Architectures/Braiding Techniques**

Two types of fiber architectures were investigated in the Technology Development Phase. The first fiber architecture was a fully braided architecture (100% braided tows) and the second architecture consisted of a triaxial braid in which longitudinal tows were in-laid among the bias tows. The fiber architectures were optimized for axial loading and shear loading [4]. The optimization process consisted of a combination of analytical parametric studies and the knowledge of braided preform manufacturing envelopes. The fiber architecture that was optimized for axial loading consisted of a triaxial braided structure containing 60% braided tows at a braid angle of  $20^\circ$  with 40% longitudinal tows; this fiber architecture is referred to as Architecture A. The fiber architecture that was optimized for shear loading consisted of a fully braided structure containing 100% braided tows at a braid angle of  $35^\circ$ ; this fiber architecture is referred to as Architecture B. A summary of the set-up variables for preform fabrication, the unit cell (fundamental repeated building block of a braided fiber architecture shown in Figure 6) characteristics of the architectures, and the preform characteristics of the architectures are found in Tables 1 and 2.



U = thickness  
 V = width  
 W = height

$\theta'$  = predetermined surface angle  
 $\theta$  = through the thickness angle  
 $\beta$  = azimuthal angle

**Braiding Ratio:**  
 $K = \frac{V}{U} = \frac{\text{track move}}{\text{column move}}$

Figure 6: Unit Cell of 3-D Braided Preform

FIBER ARCHITECTURES	A	B
<b>Manufacturing Set-up</b>		
Braided Tow Size	3K	3K
Longitudinal Tow Size	3K	NA
Number of Braiding Carriers	144	144
Number of Fixed Carriers	48	NA
Mandrel Diameter (inches)	0.96	0.96
<b>Unit Cell Characteristics</b>		
Width of Unit Cell (inches)	0.021	0.021
Length of Unit Cell (inches)	0.057	0.030
Thickness of Unit Cell (inches)	0.026	0.019
Surface Area of Unit Cell (inches**2)	1.20e-3	0.63e-3
Yarn Spacing on First Ply (inches)	0.039	0.034
Full Coverage Architecture (yes/no)	YES	YES
Amount of Spacing/Compaction (inches)	0.021	0.026
<b>Preform Characteristics</b>		
Number of Plies (inches)	5	7
Braiding Angle	20°	35°
Percentage of Braided Tows	61.5%	100.0%
Percentage of Longitudinal Tows	38.5%	0.00%
Thickness of Inner Ply (inches)	0.026	0.019
Thickness of Outer Ply (inches)	0.025	0.018
Total Thickness of Preform (inches)	0.129	0.127
Vf of Preform (%)	57.9	57.2

Table 1: Characteristics of the 2-D Braided Preforms

	TYPE 1	TYPE 2
<b>FIBER ARCHITECTURE A</b>		
Braiding Ratio	1.43	1.00
Width of Unit Cell (inches)	0.056	0.048
Length of Unit Cell (inches)	0.156	0.134
Thickness of Unit Cell (inches)	0.042	0.050
Surface Area of Unit Cell (inches**2)	8.74e-3	6.43e-3
Length of Bias Tow in Unit Cell (inches)	0.171	0.151
Through-the-Thickness Angle (degrees)	24.0	27.2
Azimuthal Angle (degrees)	35.0	45.0
<b>FIBER ARCHITECTURE B</b>		
Braiding Ratio	1.43	1.00
Width of Unit Cell (inches)	0.047	0.042
Length of Unit Cell (inches)	0.069	0.060
Thickness of Unit Cell (inches)	0.036	0.043
Surface Area of Unit Cell (inches**2)	3.24e-3	2.52e-3
Length of Bias Tow in Unit Cell (inches)	0.091	0.085
Through-the-Thickness Angle (degrees)	40.5	44.7
Azimuthal Angle (degrees)	35.0	45.0

**Specimen Type 1:** Tension, Open-Hole Tension, Compression, Bearing, CAI, Out-of-Plane Tension

**Specimen Type 2:** In-Plane Shear, Out-of-Plane Shear

**Table 2: Characteristics of the 3-D Braided Preforms**

In addition to investigating different fiber architectures, two preform fabrication techniques were investigated: 2-D braiding and 3-D braiding. All preforms used in the Technology Development Phase were manufactured to net shape. The 2-D braided materials employed for this study were formed by laminating several layers of braided fabric. The fabrics were formed with a 144 carrier braider incorporating 48 longitudinal yarns for the triaxial construction. The braids were formed on cylindrical mandrels, cut to the desired length, and stacked to achieve the desired thickness. The 3-D braiding process achieved a 3-D fully integrated fiber structure. Fibers were loaded on yarn carriers mounted on a Cartesian braiding bed. Each carrier moved in a predetermined path about the bed resulting in continuously interlaced fiber structures with no weak ply interfaces (i.e. a solid part with no layers was obtained). It is noted that the preforms contained a copper-coated graphite tracer tow. All preforms for the Technology Development Phase of the ATCAS Textile Composites Program were designed and fabricated at the Fibrous Materials Research Center at Drexel University.

## **B. Manufacturing of Braided Composites**

### **2.B.1 Fabrication of Braided Composite Specimens**

The overall manufacturing goal of the Technology Development Phase of the ATCAS Textile Composites Program was to develop a consolidation process and RTM process that consistently produced high quality braided composite test specimens. The processing challenge using the commingled AS4/PEEK material system was to achieve complete uniform wet-out of a preform made with commingled yarns. The

processing challenge of the RTM fabrication technique was to uniformly move resin through a highly interlaced structure with a high fiber volume fraction (60%). The approach taken to overcome these challenges and the optimized processing cycles is described in Reference 4.

### 2.B.2 Quality Control Procedures

The quality of the braided composite test specimens was evaluated via both destructive and non-destructive evaluation (NDE) techniques. The destructive techniques included photomicrographs and resin digestion tests; the NDE techniques included X-rays, coordinate measurements, and C-scans.

Photomicrographs were used to determine the extent of specimen wet-out, the distribution of tows throughout the composite, the percentage of longitudinal fibers in a cross-section, and the extent of fiber damage due to processing. Photomicrographs were extremely helpful in understanding the physical representation of the internal fiber architectures of the specimens. Resin digestion tests were performed (in accordance with ASTM D3171-76 [5]) to determine specimen void content and fiber volume fraction. Results from the resin digestion tests are discussed in Section 2.D. It is observed from these tests that the measured fiber volume fraction was  $60\% \pm 9\%$ .

X-rays were performed to evaluate the braid angle tolerances of the braiding process and to observe the effect of processing on the internal fiber architecture of the braided composite specimens. Measurement of the apparent braid angle from the surface of each specimen preform showed some variation between coupons and within a single coupon. Both style braids showed large variations between coupons and in some cases within individual coupons; the average braid angles varied as much as  $\pm 5.0^\circ$ . Coordinate measurements were made after fabrication to evaluate the dimensional stability of the braided composites. Dimensional stability of the RTM composite specimens was much higher than the PEEK specimens. The tolerances on the thickness of the RTM specimens were held to  $\pm 0.005$  inches as compared with  $\pm 0.025$  inches for the PEEK specimens. C-scans were performed on the braided composite specimens for NDE characterization. Ultrasonic inspection of the braided specimens generally followed conventional procedures used with laminated materials but with reduced gain. This was necessary due to the basic character of braided materials where the crossover points of the yarns in the fiber architecture are dominated by fiber properties in the thickness direction, and the open portion of the mesh is practically pure resin [6]. There is a nearly a 10 to 1 attenuation difference between these two areas on the C-scan output, causing a distinct picture of the braid pattern to be drawn during panel canning. As a result of these differences, C-scans are currently of marginal value in the NDE of braided composites; work to overcome the C-scan limitations is underway in the ATCAS Program.

Overall, the quality of the braided coupons was adequate for this initial mechanical characterization. It is expected that the first few batches of any new material will see large physical variations as methods for processing and manufacturing are developed and refined. All of the problems identified above were eliminated with manufacturing experience during the ATCAS Program; these details are discussed in the Circumferential Hoop Frame Development section of this paper.

## C. ATCAS Textile Composites Analysis (TECA)

The ATCAS Textile Composites Analysis (TECA) Model was developed to support the Technology Development and Direct Application Phases of the ATCAS Textile Composites Program. In general, TECA predicts the stiffnesses and strengths of both 2-D and 3-D braided composites under a variety of loading conditions. TECA produces a detailed description of the unit cell geometry for braided composites. The model is capable of performing analysis for a wide variety of loading conditions including: in-plane tension, in-plane compression, in-plane and transverse shear, bending, twisting, and hygrothermal loading. The model can predict the composite moduli (taking into account fiber bending and waviness), composite

Poisson's ratios, and composite coefficients of thermal expansion. TECA is also capable of producing material cards for finite element models in which complex shapes can be represented. And finally, the failure criterion contained in TECA can predict the history of failure in a braided composite. The five modules that are listed in the following section are complete. Correlation between experimental results and predicted values from TECA is ongoing; upon completion of the correlation studies, TECA will be documented in detail. The following sections describe the general content of TECA.

## 2.C.1 Model Modules

### 2.C.1.a FIBER ARCHITECTURE GEOMETRY MODULE

The analysis of textile composite structures requires the knowledge of the internal fiber architecture of the structures. The overall purpose of the Fiber Architecture Geometry Module is to produce a detailed physical representation of the fiber architecture in a braided composite structure. The types of architectures that can be represented by this module include 2-D braids, 2-D triaxial braids, 3-D braids, and woven fabrics.

The main assumption contained in this module is that one can assume that the internal fiber architecture of a braided structure can be represented by a series of repeating building blocks called unit cells. A unit cell is comprised of elemental component tows representing the braided and in-laid longitudinal tows; the physical properties of the unit cell are dependent on the manufacturing set-up and the tow characteristics. The input variables and output parameters for both 2-D and 3-D braided structures are listed in Table 3.

2-D BRAIDED ARCHITECTURE	3-D BRAIDED ARCHITECTURE
<p><b>INPUT:</b></p> <ul style="list-style-type: none"> <li>Loom Set-up</li> <li>Machine Size</li> <li>Number of Carriers</li> <li>Number of Tows per Carrier</li> <li>Mandrel Size</li> <li>Braiding Ratio</li> <li>Tow Characteristics</li> <li>Fiber Area</li> <li>Preform Characteristics</li> <li>Desired Fiber Volume Fraction</li> <li>Desired Cross-Sectional Area</li> <li>Desired Braiding Angle</li> </ul>	<p><b>INPUT:</b></p> <ul style="list-style-type: none"> <li>Loom Set-up</li> <li>Machine Size &amp; Shape</li> <li>Number of Carriers</li> <li>Number of Tows per Carrier</li> <li>Braiding Ratio</li> <li>Tow Characteristics</li> <li>Fiber Area</li> <li>Preform Characteristics</li> <li>Desired Fiber Volume Fraction</li> <li>Desired Cross-Sectional Area</li> <li>Desired Braiding Angle</li> </ul>
<p><b>OUTPUT:</b></p> <ul style="list-style-type: none"> <li>Unit Cell Dimensions</li> <li>Degree of Coverage</li> <li>Percentage of Braided Tows</li> <li>Percentage of Longitudinal Tows</li> <li>Thickness per Ply</li> <li>Final Fiber Volume Fraction</li> <li>Number of Unit Cells within a Structure</li> </ul>	<p><b>OUTPUT:</b></p> <ul style="list-style-type: none"> <li>Unit Cell Dimensions</li> <li>Angles within a Unit Cell</li> <li>Percentage of Braided Tows</li> <li>Percentage of Longitudinal Tows</li> <li>Final Fiber Volume Fraction</li> <li>Number of Unit Cells within a Structure</li> </ul>

**Table 3: Input and Output Parameters for the Preform Architecture Module**

### **2.C.1.b ELASTIC RELATIONSHIPS MODULE**

The overall objective of this module is to predict the effective elastic constants or nonlinear constitutive relationships of textile preforms for structural analysis. Non-linear response mechanisms such as shear deformation of the preform, matrix properties, and the effect of matrix cracking are taken into consideration when determining the nonlinear constitutive relationships.

The global stiffness matrix of a braided structure is calculated through the following steps: 1) the stiffness matrix for each elemental component tow is calculated through micromechanics relationships, 2) the local stiffness matrices of the elemental component tows are transformed in space to fit the composite axes, and 3) a volume averaging approach is applied to determine the global stiffnesses [7].

Stiffness modifications were introduced into the model to account for fiber bending because a tow experiences waviness around areas of interlacing and turn-around points as it traverses through a preform. The stiffnesses were modified by an elastic strain energy approach which uses beam elements to represent the bending behavior of a braided tow [4]. The total strain energy includes the strain energy due to bending and extension of the beam elements, and compression in the region of contact in tow cross-over areas.

### **2.C.1.c STRESS ANALYSIS MODULE**

Since most engineering problems are set-up for plate or shell analysis, properties are required in a form compatible with this type of analysis. The third module of TECA performs the necessary analysis utilizing the 3-D stiffness matrix determined in the previous module. First, a plane stress condition is applied (via static condensation) to the 3-D stiffness matrix. Next, integration is performed to obtain the extensional and bending stiffness matrices. Following this step, the stress field in the composite can be calculated using shear-deformable plate analysis or shell analysis.

### **2.C.1.d STRENGTH MODULE**

The overall objective of the Strength Module is to predict the history of failure of a textile composite from average stresses obtained from global structural analysis.

The Strength Module is set-up for a progressive failure analysis using the following sequence of steps: 1) the failure mechanism for the loading condition is identified, 2) the average and principal stresses and strains in the matrix are determined on a local level, 3) the matrix cracking criterion is applied via either an average stress or principal strain criterion (if matrix cracking is detected, the necessary adjustments are made to the local stress field and component stiffnesses), and 4) the failure criteria is applied via either a maximum stress or maximum strain criteria.

## **2.C.2 Support of Technology Development Activities**

The capabilities of TECA were utilized in a variety of ways in the Technology Development Phase . These roles were: fiber architecture optimization, parametric studies, material cards for finite element modelling, efficient material characterization, failure mechanism prediction, and insight to potential problem areas.

Braid pattern optimization studies were performed using TECA to aid in the development of the mechanical characterization test matrix. The analysis provided the necessary insight to which fiber architectures would be optimum for shear and axial loading [4].

TECA was also used to perform parametric studies to study the mechanical response of a wide range of fiber architectures. The model was used to relate the following: 1) composite strengths as a function of braiding angle, 2) composite moduli as a function of braiding angle, 3) the unit cell physical dimensions as a function of braiding angle and braiding ratio, 4) the coefficients of thermal expansion as a function of the unit cell geometry, and 5) design envelopes to aid designers in choosing a fiber architecture for a given ratio of in-plane to out-of-plane loading. Some of the parametric studies performed with TECA are contained in Reference 5.

TECA was also used as a tool for creating material cards for finite element modeling of braided composite tests specimens; one example of this application was the modeling of the Iosipescu test specimen [4]. TECA was also used to reduce mechanical testing and enhance data evaluation. Predicted values from TECA are currently being correlated with experimental results. If data points can successfully be correlated over a wide range of fiber architectures, TECA will be used to produce reliable predictions between correlated data points.

## D. Mechanical Characterization of Braided Composites

### 2.D.1 Objective and Test Program Issues

The overall objective of the braided composite material characterization study during the Technology Development Phase was to provide a data base of mechanical properties for development of an analytical model (TECA) and evaluation of potential applications of braided composites. Some of the more specific issues that were addressed during this study include: 1) the selection of appropriate testing procedures, 2) braided composite specimen design, 3) characterization of the mechanical response and possible failure mechanisms of braided composite material systems, 4) the effect of different fiber architectures on mechanical behavior, and 5) a comparison between the mechanical properties of braided composite systems and laminated composites (this quantified the advantages in out-of-plane strength and damage tolerance of braided composites and determined at what cost to in-plane properties these enhancements were achieved). The mechanical testing is being performed via a cooperative effort between Boeing Helicopters and the NASA Langley Research Center.

### 2.D.2 Test Matrix Identification

The test matrix assembled for the Technology Development Phase is shown in Table 4. This 114 specimen test matrix was designed to obtain a variety of data necessary for a preliminary material characterization study. The Technology Development Test Matrix was used to obtain data for braided composites consisting of two different preforms (2-D and 3-D), two different braided fiber architectures (Architectures A & B), and two different resin systems (thermoplastic - PEEK and RTM epoxy - DPL-862).

TYPE OF TEST	2-D BRAIDED SPECIMENS				3-D BRAIDED SPECIMENS			
	A		B		A		B	
	PEEK	RTM	PEEK	RTM	PEEK	RTM	PEEK	RTM
UNNOTCHED TENSION	3	6	3		3		3	3
OPEN HOLE TENSION	3	5	3		3		3	3
UNNOTCHED COMPRESSION	3	5	3		3		3	3
COMPRESSION AFTER IMPACT	3				3			
IN-PLANE SHEAR			3				3	
TRANSVERSE SHEAR			3	3			3	3
TRANSVERSE TENSION				3				5
BEARING	3	6	3		3		3	3
<b>TOTALS</b>	<b>15</b>	<b>22</b>	<b>18</b>	<b>6</b>	<b>15</b>	<b>0</b>	<b>18</b>	<b>20</b>

**NOTES:**

A - BRAIDING GEOMETRY OPTIMIZED FOR END LOAD [60% BRAIDED AT 20 DEGREES, 40% 0 DEGREES]

B - BRAIDING GEOMETRY OPTIMIZED FOR SHEAR [100% BRAIDED AT 35 DEGREES]

**Table 4: Braided Composite Technology Development Test Matrix**

In addition to the braided composite Technology Development Test Matrix, an additional test matrix was developed to directly compare the performance of braided composites with tape laminates composites. The properties that will be directly compared include: tensile strength and modulus, compression strength and modulus, in-plane shear, open-hole tension, CAI strength, and bearing strength. The lay-ups of the laminated specimens were designed to be as close as possible to the braided fiber architectures. The lay-up to simulate Architecture A was [+45/-45/0/+45/-45/0<sub>2</sub>]<sub>5S</sub> while the lay-up to simulate Architecture B was [+35/-35]<sub>17S</sub>. The material system contained in the laminated test matrix is AS4/PEEK. The testing of the specimens contained in this test matrix is currently being performed.

### 2.D.3 Specimen Configurations and Design

The unnotched tension, open-hole tension, and unnotched compression specimens were 10.00 inches long, 1.50 inches wide, and had a nominal thickness of 0.125 inches; the open-hole tension specimens had 0.25 inch diameter holes drilled through their centers. The CAI specimens were 5.00 inches long, 3.00 inches wide, and had a nominal thickness of 0.25 inches. The end edges of the specimens were ground to ensure that they were parallel prior to testing. The Iosipescu shear specimens varied in size; the length of all specimens was 3.00 inches, while the height of the specimens ranged from 0.50 to 0.75 inches and the thicknesses varied from 0.10 inches to 0.50 inches. The top and bottom surfaces (along the 3.00 inch length) of the Iosipescu specimens were also ground prior to testing to ensure dimensional accuracy. The bearing specimens were 3.50 inches long, 1.50 inches wide, and had a nominal thickness of 0.125 inches. Two 0.25 inch diameter holes were drilled through the center of the longitudinal axis 2.00 inches apart. The fasteners included 0.50 inch diameter washers which were required to perform clamp-up condition bearing tests. The specimens contained two failure sites to obtain a lower bound on the bearing strengths. The flange bending specimen was L-shaped with leg dimensions of 4.00 inches and 2.00 inches. The two critical parameters in this test method are the radius and thickness of the specimen which were 0.25 inches and 0.50 inches respectively. In order to properly design this specimen, the bending strength, in-plane strengths, and out-of-plane strength of the material must be known. At the time of test matrix identification and specimen design, these properties were not known, so the specimen configuration previously used at Boeing Helicopters with tape laminates was utilized. The procedure for future design of a flange bending specimen is outlined below:

The criterion for out-of-plane tension failure to occur before in-plane failure is:

$$\frac{\sigma_z}{\sigma_z^U} \geq \frac{\sigma_\theta}{\sigma_\theta^U} \quad (2)$$

where  $\sigma_z$  = through-the-thickness stress  
 $\sigma_z^U$  = through-the-thickness strength  
 $\sigma_\theta$  = circumferential stress  
 $\sigma_\theta^U$  = lower of in-plane compression and tension strength

Using the following isotropic relationships:

$$\sigma_z = \frac{3M}{2Rt} \quad \sigma_\theta = \frac{6M}{t^2} \quad (3)$$

where M = applied moment  
R = inner radius  
t = specimen thickness

Substituting (3) into (2) gives the following criterion :

$$\sigma_z^U \leq \sigma_\theta^U \left[ \frac{t}{4R} \right] \quad (4)$$

#### 2.D.4 Coupon Testing Procedures/Methods

All testing was performed on room temperature-dry specimens. All specimens were tested in a 50 kip MTS testing machine and ramped to failure using a constant cross-head deflection rate of 0.01 inches per minute. Failure strains and axial modulus measurements were made using strain gages and/or an extensometer. Poisson's ratio measurements were made with strain gages.

The unnotched tension and open-hole tension specimens were tested in accordance with ASTM D3039-76 [6]. The unnotched compression specimens were tested in the Boeing compression test fixture; the test fixture and method are described in detail in the Boeing Specification Support Standard BSS 7260. The compression after impact specimens were tested in the Boeing CAI compression test fixture (BSS 7260). The test specimens were first impacted at 1500 in-lbs/in with a hemispherical 0.5 inch diameter tup using a drop-weight impact testing machine and then compression loaded to failure in the test fixture. Although the specimens were impacted at 1500 in-lb/in (the Boeing specification) and the Boeing CAI test fixture was used, the specimen size was not the same as what is required in BSS 7260. The dimensions were different from the Boeing specification because the 3-D CAI specimen could not be made 4.00 inches wide at the FMRC at Drexel University. The Iosipescu shear specimen was used to test both the in-plane and out-of-plane shear specimens. The Iosipescu shear test method and test fixture are described in Reference 8; the test configuration is shown in Figure 7. A flange bending test procedure was used to conduct the testing of the out-of-plane tension specimens. One leg of radius bend specimen was securely clamped while a force was applied to the other leg creating a moment, and thus out-of-plane tension stresses, in the radius of the specimen. The flange bending test configuration is shown in Figure 7. The bearing specimens were tested in a double shear test configuration (Figure 7). The double shear test configuration was chosen because the test applies uniform bearing loads across the specimen.

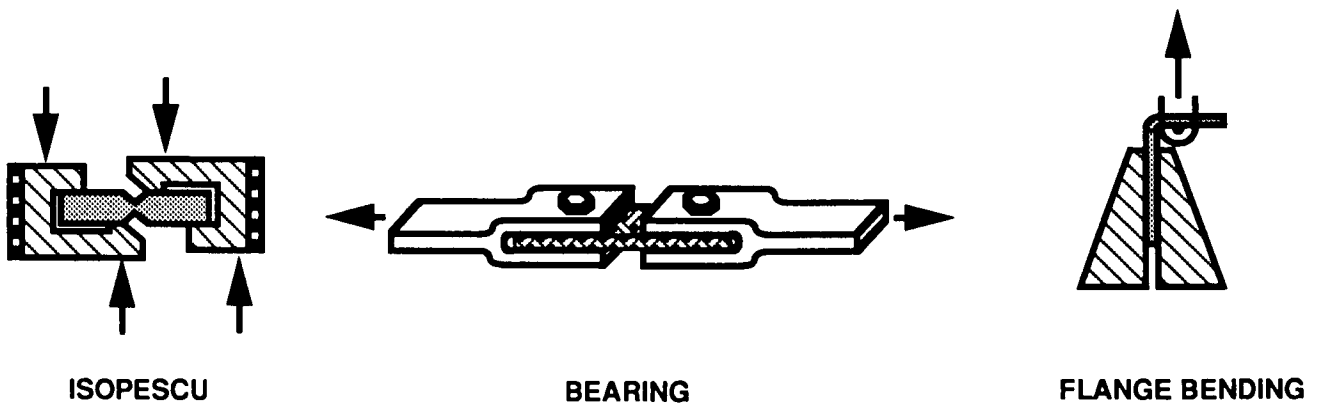


Figure 7: Braided Composite Test Specimen Configurations

#### 2.D.5 Test Instrumentation, Results , and Discussion

##### 2.D.5.a TENSION

Unnotched tension tests were performed to supply strength, modulus, Poisson's ratio, and possible failure mechanisms for the various fiber architectures tested. The specimens had (0/90) 3/16-inch long by 1/8-inch wide strain gages bonded at their mid-length. Because of the surface texture of the braided specimens,

there was an initial concern as to the accuracy of the strain gage measurements. If the gage lengths are of the same dimensional scale as the unit cell size of the braided composite, the gages may measure local variations depending on whether the gages are placed over a fiber or resin pocket. In the Technology Development Test Matrix, use of large gage sizes (as compared to the unit cell dimensions and area) were employed to ensure that the strain gage measurements averaged-out these local differences. A comparison of strain gage sizes versus unit cell dimensions for the tension tests is shown in Table 5. An extensometer was also used to measure moduli and to determine whether or not the strain gages used were sufficiently larger than the dimensions of the unit cell.

Specimen Type/Direction	Unit Cell Direction Along Gage Length (Inches)	Ratio of Gage Length to Unit Cell Dimension (Inches)
2D-A Longitudinal	0.057	3.3
2D-A Transverse	0.021	6.0
2D-B Longitudinal	0.030	6.3
2D-B Transverse	0.021	6.0
3D-A Longitudinal	0.156	1.2
3D-A Transverse	0.056	2.2
3D-B Longitudinal	0.069	2.7
3D-B Transverse	0.047	2.7

**Table 5: Strain Gage Size versus Specimen Unit Cell Size**

Results of the tension tests and average specimen fiber volume fraction and void content are summarized in Table 6. The triaxially braided architecture (Architecture A) exhibited higher tensile strength and modulus than the fully braided architecture (Architecture B) in both the 2-D and 3-D braided material systems as expected. It was observed that the in-plane tensile properties of the 3-D braided composites were significantly degraded compared with the properties of the 2-D braided composites. A summary of the reduction of in-plane tensile properties is given in Table 7. The one exception to the property degradation was the tensile modulus of the 3-D fully braided specimens which was actually 3% larger than the 2-D fully braided specimens. Moduli obtained from the strain gages and extensometer showed no significant differences in measured values indicating that the size of the strain gages was adequate; all modulus results reported in this study were calculated using a Least Squares Fit of the stress versus strain curve up to 2000 microstrain. The strain-to-failure and Poisson's ratio of Architecture B were larger than that of Architecture A due to the higher braid angle and absence of zero degree reinforcement; the Poisson's ratios were evaluated at 2000 micro strain and calculated using a secant and tangent method. The Poisson's ratio of the composites containing the DPL-862 RTM epoxy were higher than the thermoplastic braided composites. Both the 2-D and 3-D braided composites experienced high initial Poisson's ratios. The values of Poisson's ratios for the 2-D architectures ranged from 0.43 to 0.92, and the 3-D architectures ranged from 0.5 to 1.00. In general, the Poisson's ratios of braided composites, especially 3-D braided composites, tends to be higher than traditional laminated composites. It was also observed that there was a great variance in the Poisson's ratio during a test.

Specimen Type	Strength (psi)	Failure Strain ( $\mu$ Strain)	Strain Gage Modulus (Msi)	Extensometer Modulus (Msi)	Poisson Ratio (Tan/Sec )	Ave. Vf (%)	Ave. Void Content (%)
2D-A PEEK	137,900	10,300	12.96	12.61	0.562/0.533	66.3	4.1
2D-B PEEK	53,600	16,000	5.81		0.654/0.644	58.3	4.3
2D-A RTM	106,200	8,600	11.81	10.17	0.920/0.904	55.6	0.2
3D-A PEEK	109,600	9,700	10.48	10.07	0.488/0.483	59.8	3.3
3D-B PEEK	43,700	11,700	5.97		0.435/0.429	58.9	4.9
3D-B RTM	77,800	11,100	7.72	6.87	0.765/0.752	61.9	3.4

**Table 6: Braided Composite Axial Tension Test Results**

Architecture	Property	Percent of 2-D Property
Architecture A	Tensile Strength	- 20%
	Tensile Modulus	- 19%
	Compression Strength	- 10%
	Compression Modulus	- 17%
Architecture B	Tensile Strength	- 18%
	Tensile Modulus	+ 3%
	Compression Strength	- 18%
	Compression Modulus	+ 34%

**Table 7: In-Plane Properties Reduction of 3-D versus 2-D Braided Composites**

The failure surface of the braided tensile specimens was a saw-tooth pattern that propagated across the width of the specimen along a line whose shape was dependent on the length of the unit cell. The failure mechanism of the fully braided composites was a shear-out mechanism that occurred along tow boundaries. The history of failure occurred across the specimens in the following repeating sequence: 1) braided tow failure, 2) cracks forming at the broken tow boundary and propagating until a braided cross-over point, 3) failure of an intersecting tow at the cross-over point, 4) cracks forming at the intersecting broken tow boundary and propagating until the next braided cross-over point. This failure sequence was responsible for the saw-tooth pattern of the failure surface. The failure mechanism of the triaxially braided composites started with longitudinal tow failure, followed by load redistribution into the braided tows, followed by the shear-out failure just described. The failure surface of the specimens with a small unit cell length (2-D Type A and B, and 3-D Type B) propagated straight across the width of the specimens. The failure surface of the specimens with a larger unit cell length (3-D Type A) propagated diagonally across the specimen width because the cracks could propagate further along broken tows to braided cross-over points. The failure path of the AS4/DPL-862 braided composites that contained resin rich areas along the specimen

edges propagated towards these weaker areas. The saw-tooth failure pattern was also observed through-the-thickness of both the 2-D and 3-D braided composite specimens. The reason that this pattern and shear-out failure mechanism was observed through-the-thickness in the 2-D specimens was the tight nesting of fibers between braided layers.

### 2.D.5.b Open-Hole Tension

Open-hole tension tests were performed to supply strength, modulus, and failure mechanisms for the braided fiber architectures in this study. The specimens had a 3/16-inch long by 1/8-inch wide axial strain gage bonded 1.5 inches above the center of the 0.25 inch diameter hole.

Results of the open-hole tension tests and average specimen fiber volume fraction and void content are summarized in Table 8. The ultimate strength and modulus comparisons between the different fiber architectures and material system used in the study are similar to those discussed in the unnotched tension section. Test results show that the triaxially braided architecture was more notch sensitive than the fully braided architecture; this is due to the higher stress concentration of this architecture (see Table 8) and the higher strain energy release rate. Results also show that the AS4/DPL-862 epoxy material system is more notch sensitive than the AS4/PEEK thermoplastic material system; this is due to the brittle nature of the epoxy. It was also observed from the data that the 3-D braided specimens possessed a much lower notch sensitivity than the 2-D braided specimens of the same architecture. This is not due to the assumption that braided composites lower the stress concentration around a cut-out, but due to the fact that both 2-D and 3-D braided composites offer more restraint to crack propagation once local failure initiates at the edge of the hole; 3-D braided composites resist crack propagation more than the 2-D braided composites because of more fiber interlacing.

Specimen Number	Strength (psi)	Failure Strain ( $\mu$ Strain)	Strain Gage Modulus (Msi)	Percentage of Unnotched (%)	Average Vf (%)	Ave. Void Content (%)	Stress Concentration Factor
2D-A PEEK	81,700	5,600	14.61	59.3	62.1	2.2	4.60
2D-B PEEK	41,800	11,100	4.91	78.0	55.9	4.3	2.52
2D-A RTM	73,300	5,300	13.64	69.0	55.5	0.3	4.60
3D-A PEEK	67,800	5,300	13.06	73.7	60.0	3.0	4.60
3D-B PEEK	42,200	6,400	7.27	96.6	60.2	4.5	2.52
3D-B RTM	57,000	11,400	6.33	74.3	59.7	0.8	2.37

**Table 8: Braided Composite Open-Hole Tension Test Results**

The failure surface pattern of the open-hole tension specimens was the same as the failure surface pattern of the unnotched tension specimens. Failure of the open-hole specimens progressed as follows: 1) the moduli started to drop at the vicinity of the hole (plastic deformation in fully braided composites, or local tow failure in triaxial composites), 2) the local load redistributes away from the hole, followed by 3) the same failure mechanisms that were discussed in the unnotched tension section then occur.

### 2.D.5.c Compression

Unnotched compression test results were performed to supply strength, modulus, and failure mechanisms for the various fiber architectures tested. The specimens had a single axial gage bonded at their mid-length that was the same size as the gages used in the axial tension tests.

A summary of the results obtained from the compression tests along with the average specimen fiber volume fraction and void content are summarized in Table 9. The compression strength and modulus of Architecture A were much higher than that of Architecture B as expected. Similar to the in-plane tension properties, the in-plane compression properties of the 3-D braided specimens were lower than the 2-D braided specimens (Table 7). The compression strain-to-failure of Architecture B was higher than Architecture A due to the higher braid angle and absence of axial reinforcement.

Specimen Number	Strength (psi)	Failure Strain ( $\mu$ Strain)	Strain Gage Modulus (Msi)	Average Vf (%)	Ave. Void Content (%)
2-A PEEK	69,500	5,300	14.58	58.7	3.4
2-B PEEK	37,200	6,000	6.72	57.8	5.5
2-A RTM	36,300	3,400	10.90	51.4	0.3
3-A PEEK	62,300	5,600	12.04	60.9	5.1
3-B PEEK	31,400	5,600	8.99	58.7	5.5
3-B RTM	20,900	3,200	6.55	63.5	2.1

**Table 9: Braided Composite Unnotched Compression Test Results**

The failure surface of the braided compression specimens was a saw-tooth pattern that propagated straight across the width of the specimens. The failure mechanism of the fully braided composites was a shear-breakage mechanism that occurred along tow boundaries. The history of failure occurred across the specimens in the following repeated sequence: 1) braided tow waviness exerts stresses on surrounding matrix causing cracking along the tow boundary, 2) localized fiber-matrix debonding 3) the fiber tow fails due to compression and/or localized bending, 4) matrix crack propagates along broken tow boundary until a braided cross-over point, 5) failure of an intersecting tow at the cross-over point, and 6) cracks form at the intersection broken tow boundary and propagate until the next braided cross-over point. The failure mechanism of the triaxially braided composites occurred in the following sequence: 1) longitudinal fibers exert stresses on the surrounding matrix causing cracking, 2) localized fiber-matrix debonding, 3) fiber tow failure due to compression and/or localized bending, 4) load redistribution into the braided tows, and 5) the shear-breakage failure just described. The triaxially braided specimens did not exhibit the brooming failure observed in traditional laminates because the longitudinal tows are tightly nested within the architecture. The saw-tooth failure pattern was also observed through-the-thickness of both the 2-D and 3-D braided composite specimens. As with the 2-D braided tensile specimens, this shear failure mechanism was observed through-the-thickness because of the tight nesting of fiber tows between braided layers. The delaminations inherent to laminated composite compression specimens were not observed because of the nesting. The global delaminations and sub-laminate buckling that contribute to laminated composite

compression failure did not occur in the 2-D braided composites. Local delaminations in the 2-D braided composites did not propagate beyond the unit cell level.

#### 2.D.5.d Shear

Iosipescu shear tests were performed to measure the in-plane and out-of-plane shear stiffness and strength of the braided material systems.

The specimens had (0/± 45) 1/16-inch long by 1/16-inch wide strain gages bonded in the test section back-to-back. Gages this size had to be used because of the dimensions of the Iosipescu shear specimen configuration. The gages were not larger than the characteristic dimensions of the unit cell for the Iosipescu test specimens and thus measured local variations depending on whether the gage was applied over a fiber or resin pocket. After analyzing strain gage data, it was concluded that an initial shear modulus is the only braided composite property that can be measured with the Iosipescu shear test. The technique of calculating initial modulus is itself questionable; it is obtained by averaging the readings of four strain gages (± 45° gages on the front and back of the specimens); the in-plane and out-of-plane shear data is not included because of this uncertainty. The following characteristics of the Iosipescu shear test method make it unattractive for shear testing of braided composites: the specimen has a small test section which requires small gages which do not measure the degree of homogeneity that is desired, the specimen edges must be ground so they are perfectly parallel, the load path changes during loading in both the longitudinal and transverse directions, a stress gradient exists across the width (i.e. through-the-thickness effects) which is not taken into consideration, and coupling exists due to material anisotropy.

#### 2.D.5.e Out-of-Plane Tension

Flange bending tests were performed to measure the out-of-plane tension failure stresses and to observe failure mechanisms of the braided material systems.

A summary of the results from the out-of-plane tension tests is given in Table 10. The transverse strengths shown in the table were calculated using isotropic methods (equation 3); calculations using curved composite methods are currently being performed. The results show that both 2-D and 3-D braided material systems exceed the out-of-plane tension strengths of quasi-isotropic tape laminates; a comparison of the transverse tension strengths can be found in Figure 8. Justification for the high transverse tension strength in the 2-D braided specimens stems from the fact that the braided layers of the 2-D braided specimens are nested tightly together and do not have resin rich inter-ply planes through which cracks easily propagate. Some through-the-thickness reinforcement provided by the inter-ply nesting and fiber crimp also aided in the out-of-plane strength. The high percentage of through-the-thickness tows is justification for the high transverse tension strength in the 3-D braided specimens.

Specimen Number	Failure Load (lb)	Moment (In-lb)	Strength (psi)	Average Vf (%)	Ave. Void Content (%)
2D-A RTM	720	690	8,450	64.1	0.6
3D-B RTM	600	718	> 8,610	64.1	1.9

Table 10: Braided Composite Out-of-Plane Tension Test Results

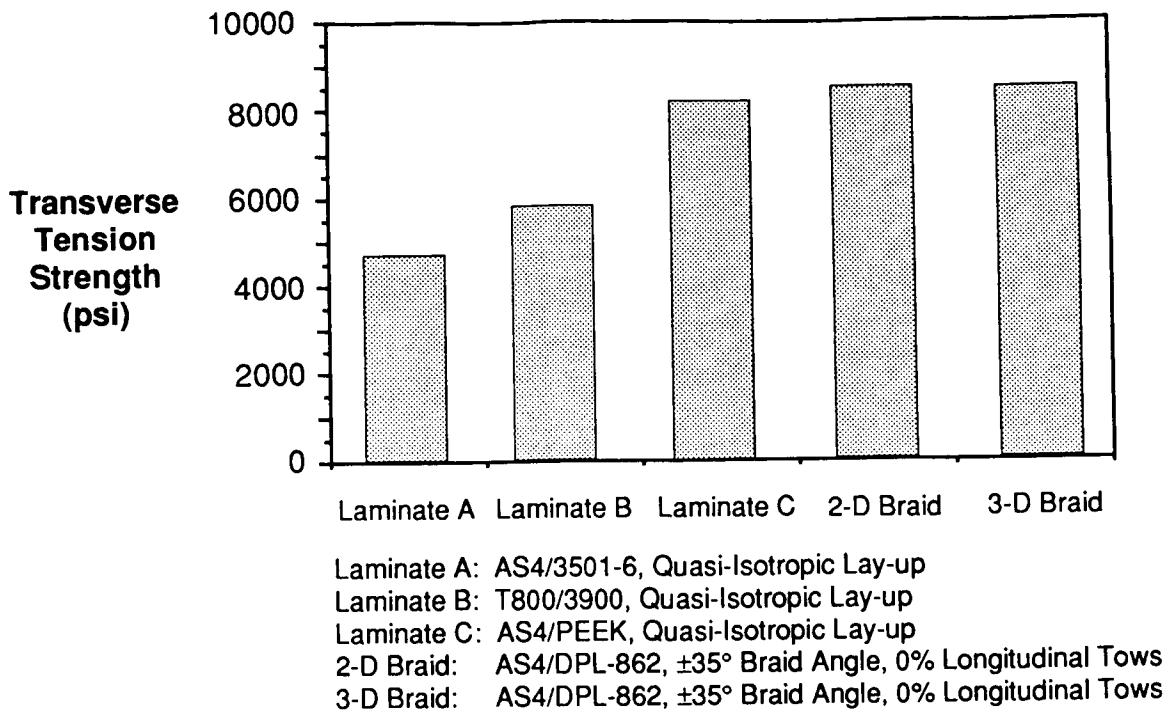


**Figure 8: Transverse Tension Strength Comparison of Braided and Laminated Composites**

The 2-D braided specimens failed in an out-of-plane tension failure mode. The first crack to appear in the 2-D braided specimens was a circumferential crack found between braided plies at a distance approximately 40% of the bend thickness measured from the inner radius; this is the location of maximum radial stress [9]. This crack propagated until the strain energy release rate dropped below the critical strain energy release rate needed to propagate the crack. Once crack propagation has stopped, the thickness can be viewed as two sub-laminates each having a peak stress. Theoretically the peak stress on the inner sub-laminate is greater than the peak stress of the outer [9]. Experimental results of this study contradict this theory because immediately following load redistribution, a second circumferential crack appeared in the middle of the outer sub-laminate. It is believed that the location of the second crack is dependent on the fiber architecture configuration and material anomalies (i.e. resin rich areas). Due to the nature of the manufacturing process used to fabricate the braided specimens, the fiber volume fraction is greater in the inner sub-laminate than the outer possibly explaining why the second crack appeared at this location in the specimens used in this study. The 3-D braided test specimens experienced in-plane failure due to bending and not an out-of-plane tension failure mode; this was due to the large amount of through-the-thickness fibers (and thus strength) in the specimens and the inadequate strength of the composite in the circumferential direction (i.e. equation 4 was violated). The 3-D out-of-plane tension specimens could not be designed properly due to the lack of braided composite material properties that were available at the time of specimen design. Failure of the 3-D braided specimens was in the form of transverse cracking along the inner radius of the bend.

#### 2.D.5.f Compression After Impact

Damage size and post-impact strength were measured in compression-after-impact tests. CAI tests were performed on 2-D and 3-D triaxially AS4/PEEK braided specimens.

C-scans of the impacted specimens were performed to observe the shape and extent of damage. The shape of the damage area for both the 2-D and 3-D braided specimens were similar. All specimens possessed an elliptical damage area with extensive back-side fiber break-out damage; the fiber break-out damage was dome-shaped. The damage was elliptical due to the high axial stiffness of the specimens. The elliptical

damage area of the 2-D braided specimens extended to the clamped boundary conditions along the 5.00 inch length. The damage area of the 3-D braided specimens was not as severe as the 2-D braided specimens for the following reasons: 1) the through-the-thickness reinforcement and the tightly interlaced structure prevented crack propagation and delaminations, and 2) the reduced in-plane stiffness of the 3-D architecture reduced the peak impact force during impact.

A summary of the results obtained from the CAI tests along with the average specimen fiber volume fraction and void content are summarized in Table 11. The average CAI strength of the 2-D braided specimens was 49 ksi (~ 71% of the undamaged compression strength) while the average CAI strength of the 3-D braided specimens was 58 ksi (~ 92% of the undamaged compression strength). A comparison of CAI strengths between the braided material systems and three quasi-isotropic laminated tape material systems is shown in Figure 9.

Specimen Number	Strength (psi)	Percentage of Unnotched (%)	Average Vf (%)	Average Void Content (%)
2D-A PEEK	49,000	70.5	60.3	3.1
3D-A PEEK	57,700	92.6	61.2	3.9

Table 11: Braided Composite Compression After Impact Test Results

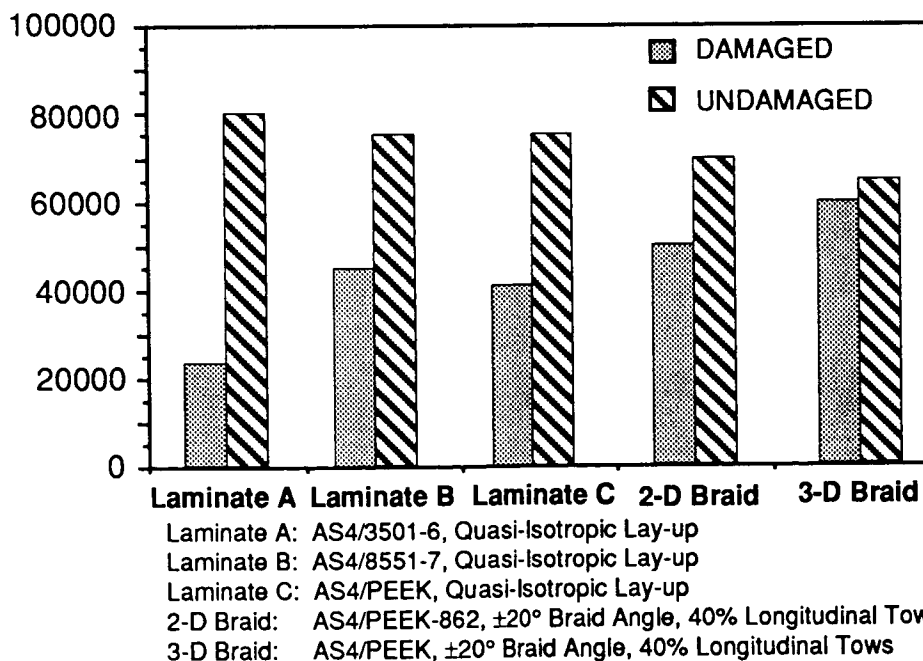


Figure 9: CAI Strength Comparison of Braided and Laminated Composites

The failure surface pattern of the CAI specimens was the same as the unnotched compression specimens. The curvature of the dome area and the small area of fiber breakage reduced the stiffness across the damage area causing some load to be redistributed into the undamaged region and thus increasing stresses around the damage site. Failure initiated in the damaged area of the specimens by a combination of the in-plane

stress concentration and localized bending moment in the fiber break-out dome area, although the bending deformation that occurred in the dome area contributed more to the initiation of failure than the stress concentration. Failure initiated on the inside (concave surface) of the dome because the compression and bending stresses are superimposed to give the maximum stresses in the damage area. Global failure of the CAI specimens occurred through a shear-breakage mechanism that occurred along tow boundaries. The complete failure mechanism of the CAI specimens was the same as the unnotched compression specimen previously discussed. The excellent performance of both the 2-D and 3-D braided specimens was caused by the interlaced structure which prevented both delamination and back fiber pull-out across the whole length of the specimen (i.e. the fibers are constrained from pulling free at the braid crossover points) as in the case with conventional laminates. Once again, local delaminations in the braided composites did not propagate beyond the unit cell level.

#### 2.D.5.g Bolt Bearing

Bearing tests were performed using a zero clamp-up condition to supply bearing strength data for the various fiber architectures.

A summary of results obtained from the bolt bearing tests is given in Table 12. The bearing strength of Architecture A was greater than that of Architecture B for all material systems tested. The low bearing strength of Architecture B was caused by the lack of longitudinal fibers. The bearing strength of the AS4/PEEK braided material systems was higher than the bearing strength of the AS4/DPL-862 braided material system; the lower compression strength of the RTM epoxy and areas of resin richness around the drilled holes are possibly accountable for the lower bearing strength. In comparing the 2-D and 3-D braided composites, the 3-D braided specimens exhibited a higher bearing strength than the 2-D braided specimens with the same fiber architecture; this was due to a larger percentage of fibers tangential to the fastener hole in the 3-D braided systems. Overall, the braided specimens tested during this study exhibited poor ultimate bearing strengths as compared to tape laminates; ultimate stresses ranged from 40 ksi to 60 ksi (compared 110 ksi for quasi-isotropic tape laminates). The poor performance of these specimens was caused by braided preform characteristics, fiber architecture, preform quality, and resin rich areas in the vicinity of the fasteners. In general, bearing strengths of textile composites do not compare favorably with the bearing strengths of tape laminated composites because of the excessive fiber crimp in the textile preform. In addition to fiber crimp, the shallow braid angles of architectures A and B offered little resistance to fastener movement. It is noted that these fiber architectures were not optimized for bearing strength.

Specimen Number	Failure Load (lb)	Bearing Strength (psi)	Average Vf (%)	Average Void Content (%)
2-A PEEK	1,840	63,960	61.2	3.3
2-B PEEK	880	49,820	60.2	5.2
2-A RTM	1,550	47,540	53.6	0.5
3-A PEEK	2,300	71,600	65.1	5.8
3-B PEEK	1,760	55,600	59.9	5.1
3-B RTM	1,360	42,360	54.5	5.7

Table 12: Braided Composite Bolt Bearing Test Results

The failure mechanism for each specimen tested was a brooming failure directly outside of the fastener hole. The geometry of the washers restricted the failure mode directly around the hole.

### 2.D.6 Preliminary Correlation between Experimental Results and Analysis

Correlation between experimental data and analytical predictions from TECA is underway. Net-shape tension and compression data from the Braided Composite Technology Development Matrix were correlated for both the 2-D and the 3-D AS4/PEEK braided material systems. Correlation of the experimental data obtained for the AS4/DPL-862 braided materials systems has not begun because sufficient data has not been obtained for the RTM resin system. A test plan to obtain the necessary resin properties for analytical model input is currently being conducted.

Results from the preliminary correlation studies are shown in Figure 10. The TECA predicted values are within 6% of the tensile strength data and 9% of the compression strength data; the predicted values for the tensile and compression moduli are both within 5% of the measured values.

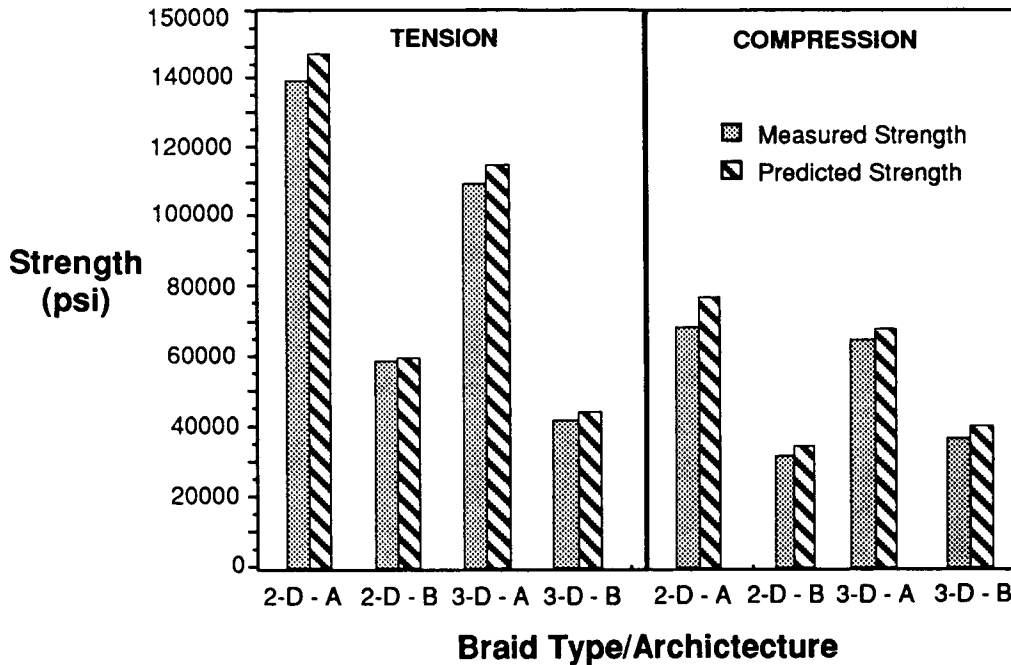


Figure 10: Correlation Between Experimental Results and TECA Predicted Values

## 3. CIRCUMFERENTIAL HOOP FRAME DEVELOPMENT

### A. Material Selection

The RTM resin system used in the Technology Development Phase was not used in the development of the circumferential hoop frames. The structural properties of the DPL-862 resin system, specifically the room temperature/dry compression and hot-wet compression performance, were not acceptable for commercial aircraft applications. However, it is noted that DPL-862 did serve its purpose in RTM process development and the initial screening of the mechanical performance of braided composites. After a detailed comparison study of various RTM resin systems from Shell, 3M, Dow, and British Petroleum, Shell's 1895 resin with curing agent W was chosen. The 1895 resin system costs \$12.50/lb, its structural performance is slightly better than 3501-6, and its viscosity profile is suitable for RTM. It is also noted that this resin system possesses a high glass transition temperature (420°F) which produces high hot-wet retention properties and is necessary for co-bonding precured structures. The combined AS4/1895 material system cost is approximately \$21/lbs (waste not included).

## B. Frame Fiber Architecture Design

As discussed in Section 1.B.2, the ultimate pressure loading condition is the most critical loading condition for the circumferential hoop frames located in the crown panel. Using the ATCAS design criteria, the minimum axial stiffness of the frames was determined to be 6.6 Msi (based on loads as of 2/91). TECA was then utilized to produce a tensile modulus design space (Figure 11) for the triaxially braided/RTM material system as a function of percentage of longitudinal tows and braiding angle; the design space provided an envelope of valid fiber architectures for a 55% fiber volume fraction. Once the design space was defined, other critical design issues inherent to the circumferential hoop frames were addressed. These critical issues included: thermal dimensional stability, mouse hole cut-outs, out-of-plane tension strength, bearing performance, and damage tolerance. Using the design space and taking into consideration the critical design issues listed above, the frame fiber architecture was chosen to consist of 37.5% longitudinal fibers with a braid angle of 66.5°; this fiber architecture is referred to as the "B1" or the "frame" architecture. Six plies of this braided fabric were used to produce a thickness of 0.141 inches. This architecture consists of 6K size tows which were chosen because they are easy to braid and produce preforms with high inter-ply nesting.

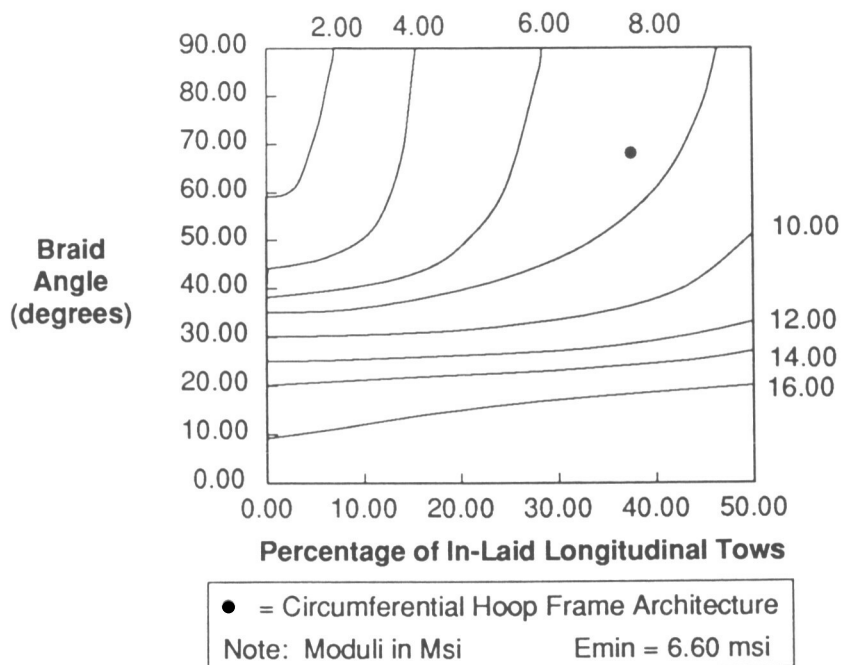


Figure 11: TECA Tensile Modulus Design Space

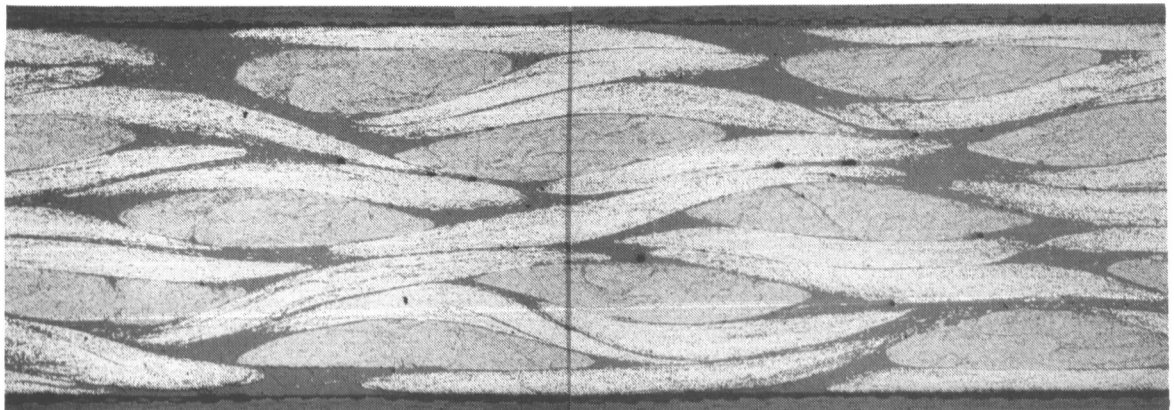
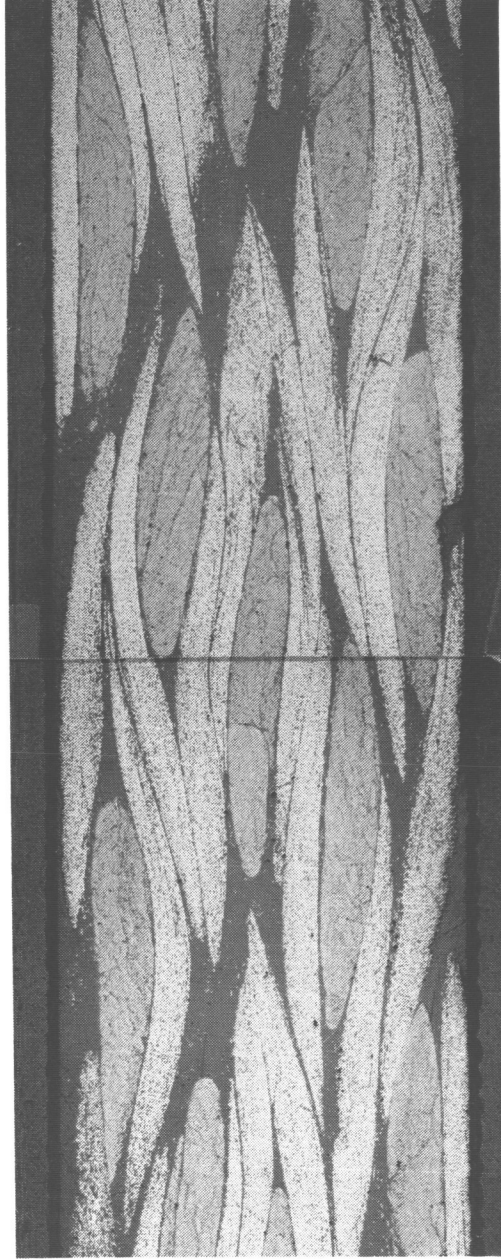


Figure 12: Cross-Section of Circumferential Hoop Frame Architecture



**Figure 13: Cross-Sections of Alternate Circumferential Hoop Frame Architectures  
(top: Architecture A1, bottom: Architecture B2)**

**Table 13: Characteristics of the 2-D Triaxially Braided Preforms**

<b>Fiber Architecture</b>	<b>A 1</b>	<b>B 1</b>	<b>B 2</b>
<b>Manufacturing Set-up</b>			
Braided Tow Size	12K	6K	6K
Longitudinal Tow Size	24K	18K	18K
Number of Braiding Carriers	144	144	144
Number of Fixed Carriers	72	72	72
Mandrel Diameter (inches)	5.50	4.80	5.25
<b>UNIT CELL Characteristics</b>			
Width of Unit Cell (inches)	0.120	0.105	0.115
Length of Unit Cell (inches)	0.061	0.046	0.042
Thickness of Unit Cell (inches)	0.037	0.026	0.027
Surface Area of Unit Cell (inches**2)	7.32e-3	4.83e-3	4.83e-3
Yarn Spacing on First Ply (inches)	0.109	0.084	0.078
Amount of Spacing/Compaction (inches)	0.011	0.006	0.012
<b>Preform Characteristics</b>			
Number of Plies (inches)	4	5	5
Braiding Angle	63°	66.5°	70°
Percentage of Braided Tows	68.8%	62.6%	66.1%
Percentage of Longitudinal Tows	31.2%	37.4%	33.9%
Thickness of Inner Ply (inches)	0.037	0.026	0.027
Thickness of Outer Ply (inches)	0.036	0.026	0.026
Total Thickness of Preform (inches)	0.146	0.131	0.132
Vf of Preform (%)	54.3	54.2	54.3

A photomicrograph of the frame architecture is shown in Figure 12. Two alternate architectures were identified so that the ATCAS DBT could promptly respond to future design criteria changes and/or unforeseen preform fabrication difficulties. The additional architectures will also provide a larger data base for TECA correlation. The first alternate architecture, B2, consists of 6K tows and contains 34% longitudinal fibers with a braid angle of 70°. The second alternate architecture, A1, consists of 12K tows and contains 31% longitudinal fibers with a braid angle of 63°. Photomicrographs of the two alternate fiber architectures are found in Figure 13. A summary of the set-up variables for preform fabrication, the unit cell characteristics of the architectures, and the preform characteristics are shown in Table 12; the values contained in this table were obtained using TECA.

### **C. Manufacturing of Braided Composite Specimens**

The manufacturing of the braided composite specimens and the 3 ft frames for the manufacturing demonstration during the Direct Application Phase was performed at Fiber Innovations Inc. (FII). Braided composite manufacturing technology developed at Boeing, FII, and Shell Chemical Co. was jointly utilized during this Phase of the ATCAS Program.

#### **3.C.1 Preform Fabrication**

All preforms were formed with a 144 carrier New England Butt triaxial braider incorporating 72 longitudinal yarns in a 2/2 regular braid pattern. The preforms were formed on cylindrical mandrels and the desired preform thickness was achieved by over-braiding layers. To verify the placement of yarns in the structure, each preform was formed with one longitudinal and one braided nickel coated AS-4 carbon tracer yarn. Following braiding, the preform was cut longitudinally and removed from the mandrel. The preforms were then stabilized along the perimeter with Kevlar stitching thread to prevent the plies from shifting or distorting during insertion into the mold and also to reduce the potential for fiber wash-out during RTM.

#### **3.C.2 Resin Transfer Molding**

The RTM process at FII involves a combination of pressure and vacuum. FII has expended considerable time and energy to gain knowledge and experience in perfecting their own version of the RTM process. The details of the RTM process with the 1895 resin system are discussed in Section 3.E.2.

The target thickness tolerance of the braided composite specimens was  $\pm 0.010$  inches; the target fiber volume was 55% with a  $\pm 5\%$  variation, the tolerance of all radii was  $\pm 0.01$  inches; and the tolerance on braid angle was  $\pm 2.5^\circ$ .

#### **3.C.3 Quality Control Procedures**

The quality of the braided composite test specimens involved in the Direct Application Phase was evaluated using the same procedures as in the Technology Development Phase. The results of the quality assessment evaluations are summarized below.

Photomicrographs of the specimens showed the triaxially braided preforms were completely wet-out during the RTM process (Figure 12 and 13). The photomicrographs also showed uniform distribution of the in-laid longitudinal tows and a high degree of inter-ply nesting. Resin digestion tests proved that the braided preforms were completely wet-out; the void content of all the braided composites tested so far is under 0.5%. The fiber volume fraction of the composites was also determined via the resin digestion tests and showed that the fiber volume fractions were within the specified tolerances.

By tracing the nickel coated tracer yarns, the braid angle was measured for each of the specimens. The variation of braid angle within and between the braided composites was negligible and well within the specified tolerances. However, there was a slight variation in thickness from specimen to specimen. This

was due to the fact that two panels were RTM simultaneously and that the tool cavities were not identical. Although there is a slight variation, the dimensions of the specimens are all within the specified tolerances.

## D. Material System Performance Evaluation

### 3.D.1 Test Program Objectives

The overall objective of the braided composite material characterization study during the Direct Application Phase was to provide a data base of mechanical properties to support the preliminary design of the crown panel circumferential hoop frames. The test matrix is also being used to add to the existing braided composite data base and to further characterize the structural performance of braided composites.

### 3.D.2 Test Matrix Identification

The test matrix assembled for the Direct Application Phase is shown in Table 14. The test matrix contains three fiber architectures: the chosen frame architecture "B1", and the two alternate architectures, "A1" and "B2", whose braid angle and percentage of in-laid longitudinal fibers vary from the frame architecture.

TYPE OF TEST	FIBER ARCHITECTURES			TOTALS FOR TEST TYPE
	A1	B1	B2	
1 TENSION	3	3	3	9
2 OPEN-HOLE TENSION	3	3	3	9
3 COMPRESSION	3	3	3	9
4 OPEN-HOLE COMPRESSION	3	3	3	9
5 IN-PLANE SHEAR	4	4	4	12
6 OUT-OF-PLANE TENSION	5	5	5	15
7 COMPRESSION AFTER IMPACT	6	6	6	18
8 TENSION AFTER IMPACT	2	2	2	6
9 BEARING	8	8	8	24
10 FATIGUE	12	12	12	36
11 TENSION (UNCUT EDGES)	4	4	4	12
12 TRANSVERSE TENSION	6	6	6	18
13 WIDTH-EFFECT TENSION	0	0	12	12
14 FATIGUE (UNCUT EDGES)	0	2	0	2
15 OUT-OF-PLANE SHEAR	TBD	TBD	TBD	TBD
16 HOT-WET COMPRESSION	4	4	0	8
<b>TOTALS FOR ARCHITECTURE</b>	<b>63+</b>	<b>65+</b>	<b>71+</b>	<b>199+</b>

**Table 14: Braided Composite Direct Application Test Matrix**

In addition to providing in-plane and out-of-plane strength, stiffness, and fatigue properties, this test matrix also provides an indication of how a new material would be expected to function in a structural application. The open-hole tension and compression tests provide an indication of the material's tolerance to imperfections. The damage tolerance tests measure the material's response to impact loading and resistance to impact damage and can be used as a rough measure of thickness-direction strength. The bolt bearing data provides important parameters in structural applications where mechanical fasteners are used.

### 3.D.3 Specimen Configurations and Design

The following specimens had the same configurations as the tension specimens discussed in the Technology Development section: tension, open-hole tension, transverse tension, width-effect tension (with widths of 1.0, 2.0, 3.0, and 4.0 inches), compression, open-hole compression, hot-wet compression, and fatigue. The in-plane shear test will be a rail shear test; the test fixture for this test is currently being designed. The out-of-plane shear specimen configuration is currently under investigation. The out-of-plane tension specimen is a flange bending specimen whose configuration is identical to the circumferential hoop frame configuration. The compression after impact specimens are 6.0 inches long, 4.00 inches wide, and have a nominal thickness of 0.25 inches. The tension after impact specimens are 10.00 inches long, 4.00 inches wide, and have a nominal thickness of 0.125 inches. The specimens used for the bearing tests have the same design as discussed in the Technology Development section.

### 3.D.4 Coupon Testing Procedures/Methods

All testing is being performed on room temperature-dry specimens. All specimens are being tested in a 50 kip MTS testing machine and are being ramped to failure using a constant cross-head deflection rate of 0.05 inches per minute. The procedures discussed in the Technology Development section have been used in the tests that have been completed during the Direct Application Phase.

### 3.D.5 Test Instrumentation, Results, and Discussion

The testing involved with the Direct Application Test Matrix is on-going. The following sections will summarize the results that have been obtained so far. The failure mechanisms of the test specimens will be reported in a further publication. Tests that have been completed include: tension, transverse tension, compression, open-hole compression, hot-wet compression, out-of-plane tension, and bearing.

#### 3.D.5.a Tension

Unnotched tension tests were performed to supply strength, modulus, and Poisson's ratios for the 3 architectures involved in this study. The specimens had (0/90) strain gages of different sizes (1/16 inch, 1/8 inch, and 3/16 inch) bonded at their mid-length; an extensometer was also used to measure strain. The 1/16 inch and 1/8 inch strain gages were square and the 3/16 inch gage was 1/8 inch wide. A variety of strain gage sizes were used to observe the effect of strain gage size versus unit cell size. A comparison of strain gage sizes versus unit cell dimensions for the tension tests is shown in Table 15.

Architecture/ Direction	Unit Cell Dimension (inches)	Ratio of 1/16 inch Gage Length/ Unit Cell Dimension	Ratio of 1/8 inch Gage Length/ Unit Cell Dimension	Ratio of 3/16 inch Gage Length/ Unit Cell Dimension
B1 Longitudinal	0.046	1.4	2.7	4.1
B1 Transverse	0.105	0.6	1.2	1.8
B2 Longitudinal	0.042	1.5	3.0	4.5
B2 Transverse	0.115	0.5	1.1	1.6
A1 Longitudinal	0.061	1.0	2.1	3.1
A1 Transverse	0.120	0.5	1.0	1.6

Table 15: Strain Gage Size versus Specimen Unit Cell Size

Results of the tension tests are summarized in Table 16. The B1 architecture possessed the highest strength and stiffness values; this was caused by the higher percentage of in-laid longitudinal tows in this architecture compared to the A1 and B2 architectures. Moduli obtained from the 1/8 inch and 3/16 inch strain gages and extensometer showed no significant differences in measured values (all moduli results reported in this study were calculated using a Least Squares Fit of the stress versus strain curve up to 2000

microstrain). This observation was expected because the gage lengths were sufficiently larger than the unit cell dimension in the loading direction. The moduli obtained from the 1/16 inch gages varied from the other gages and extensometer. The variation is due to the gage length being of the same dimensional scale as the length of the unit cell; gage lengths similar to unit cell dimensions are sensitive to localized effects within the unit cell. A wide range of Poisson's ratios was measured with the different size strain gages (the Poisson's ratios were evaluated at 2000 microstrain and calculated using a tangent method); this measurement is also sensitive to gage length versus unit cell size. The 1/16 inch and 1/8 inch gages oriented in the transverse direction were of the same dimensional scale as the unit cell width and were sensitive to localized effects. The 3/16 inch gage oriented in the transverse direction was sufficiently larger than the unit cell width and measured more accurate values.

Specimen Architecture	Stress (Ksi)	1/16 Inch Gage Modulus (Msi)	1/8 Inch Gage Modulus (Msi)	3/16 Inch Gage Modulus (Msi)	Extensometer Modulus (Msi)	1/16 Inch Gage Poisson's Ratio	1/8 Inch Gage Poisson's Ratio	3/16 Inch Gage Poisson's Ratio
A1	62.6	7.10	6.35	6.51	6.61	0.264	0.225	0.300
B1	80.7	7.18	6.94	6.88	6.72	0.186	0.185	0.268
B2	57.1	6.30	6.32	6.30	6.66	0.165	0.151	0.183

**Table 16: Braided Composite Axial Tension Test Results**

### 3.D.5.b Transverse Tension

Unnotched transverse tension tests were performed to supply strength, modulus, and Poisson's ratios. The same strain measurement techniques described for the unnotched tension specimens were utilized for the transverse tension tests.

Results of the transverse tension tests are summarized in Table 17. The B2 architecture possessed the highest strength and stiffness values; this is due to the higher braiding angle in this architecture as compared to the A1 and B1 architectures. Moduli obtained from the strain gages and extensometer showed variability in measured values. The variability was caused by the gage lengths being smaller or of the same dimensional scale as the length of the unit cell in the loading direction (see Table 15). The 3/16 gage showed the least amount of variability within specimens containing this size gage because it was approximately 1.5 times the unit cell dimension. A factor of 1.5 is most likely the minimum in choosing a strain gage size for accurate measurements of braided composites (thorough studies to determine the minimum factor are on-going). Similarly to the unnotched tension tests, a wide range of Poisson's ratios was measured with the different size strain gages because the gages were not of sufficient size; the 3/16 inch gage exhibited the least amount of variability in the testing.

Specimen Architecture	Stress (Ksi)	1/16 Inch Gage Modulus (Msi)	1/8 Inch Gage Modulus (Msi)	3/16 Inch Gage Modulus (Msi)	Extensometer Modulus (Msi)	1/16 Inch Gage Poisson's Ratio	1/8 Inch Gage Poisson's Ratio	3/16 Inch Gage Poisson's Ratio
A1	32.25	6.58	6.59	6.24	5.78	0.225	0.280	0.307
B1	41.7	7.45	6.13	6.80	6.45	0.291	0.163	0.199
B2	45.5	7.35	7.18	7.11	7.26	0.161	0.188	0.190

**Table 17: Braided Composite Transverse Tension Test Results**

### 3.D.5.c Compression

Unnotched compression tests were performed to supply strength, modulus, and Poisson's ratios for the various fiber architectures tested.

A summary of the results obtained from the compression tests are summarized in Table 18. Architecture B1 possessed the highest strength of the three architectures tested because of the higher percentage of longitudinal fibers in the B1 architecture.

Specimen Architecture	Failure Stress (psi)	% Unnotched
<b>Unnotched</b>		
A 1	44,626	----
B 1	73,634	----
B 2	56,508	----
<b>Open-Hole</b>		
A 1	43,972	99
B 1	52,399	71
B 2	45,150	80

**Table 18: Braided Composite Compression Test Results**

### 3.D.5.d Open-Hole Compression

Open-hole compression tests were performed to supply strength and modulus of braided compression specimens containing imperfections.

Results of the open-hole compression tests are summarized in Table 18. Although the B1 architecture possessed the highest notched compression strength, it also experienced the largest knock-down of the unnotched compression strength as compared to the B2 and A1 architectures. The high open-hole compression strength was due to the high percentage of longitudinal fibers. The difference in the notch sensitivity of the three architectures appears to be related to the unit cell dimensions of the architectures, specifically the longitudinal tow separation. It is speculated that if the unit cell dimensions are of the same dimensional scale as the stress concentration distribution area, different failure mechanisms occur because of increased interaction between braided and longitudinal tows thus lowering notch sensitivity. The topic of notch sensitivity as a function of unit cell size is currently being thoroughly investigated.

### 3.D.5.e Hot-Wet Compression

Hot/wet compression tests were conducted (at 180°F and 100% relative humidity after a 30 day soak) to determine the environmental effects on the crown frame material system (Architecture B1). Results of these tests show a 26.5% reduction in compression strength from room temperature/dry which is slightly better than 3501-6 hot/wet compression performance.

### 3.D.5.f Out-of-Plane Tension

Flange bending tests were performed to measure the out-of-plane tension failure stresses of the braided frame material system and configuration.

A summary of the results from the out-of-plane tension tests are given in Table 19. The transverse strengths shown in the table were calculated using the isotropic methods discussed in the Technology Development section. The results show that that the 2-D braided material system exceeds the out-of-plane

strength of quasi-isotropic tape laminates (see Figure 8). Justification for the high transverse tension strengths is discussed in the Technology Development section. Architecture A1 did not fair as well as Architectures B1 and B2 because the 12K tows do not nest as well as the 6K tows (see Figures 12 and 13).

Specimen Architecture	Failure Load (lb)	Moment (In-lb)	Strength (psi)
B1	199	223	9,486
B2	205	230	9,772
A1	157	176	7,484

**Table 19: Braided Composite Out-of-Plane Tension Test Results**

### 3.D.5.g Bolt Bearing

Bearing tests using a zero clamp-up, 35 in-lb torque, and 90 in-lb torque condition were performed to determine bearing strengths for the three architectures involved in this study.

A summary of results obtained from the bolt bearing tests is given in Table 20. The bearing stresses of the specimens contained in the Direct Application Test Matrix were much higher than the specimens previously discussed in the Technology Development Test Matrix. With a no-clamp-up condition, the bearing strengths of the 3 architectures contained in this study ranged from 90 ksi to 100 ksi. The increase in bearing strength of these braided composites can be attributed to the high percentage of axial tows, high braid angles, good preform quality, and excellent composite quality. The high braid angle provided higher tangential stiffness and restrained bearing deformation, the straight longitudinal fibers also restricted movement, and the absence of resin rich areas around the hole prevented premature yielding. The application of 35 in-lb of torque increased the bearing ultimate strengths by approximately 20% over the zero clamp-up condition while the full torque condition (90 in-lb) increased the ultimate stresses by approximately 30%. Enhanced performance of the clamp-up tests was attributed to the friction force created by torquing the fastener.

Specimen Architecture	Torque (in-lb)	Ultimate Load (lb)	Bearing Strength (Ksi)
A1	0	3047	89.050
	35	3795	115.560
	90	4360	128.716
B1	0	3465	99.155
	35	4003	119.235
	90	4480	129.841
B2	0	3315	95.568
	35	3908	114.100
	90	4139	118.243

**Table 20: Braided Composite Bolt Bearing Test Results**

## E. 3 ft Frame Manufacturing Demonstration

The fabrication of the twelve 3 ft. frames were used to achieve the following objectives: 1) to demonstrate the proof of manufacturing concept and requirements defined in global evaluation, 2) to demonstrate batch mode processing, 3) to determine tooling and manufacturing modifications that improve part quality and producibility, 4) to assist in the local optimization of the frame configuration, and 5) to identify and address

potential problem areas that affect scale-up. The following sections describe the manufacturing details that were used to fabricate the 3 ft demonstration frames.

### 3.E.1 Manufacturing of Different Structural Configurations

Four frame configurations consisting of different combinations of flange caps and filler packs were fabricated during the manufacturing demonstration to gain manufacturing experience and to aid the design optimization; each combination is described in Table 21. More specifically, the configurations were fabricated to optimize the frame cost benefits, manufacturing process, and structural performance. Two types of radius filler packs (Narmco 1515 adhesive and dry braided fiber) and two bottom flange cap configurations (braided cap and no cap) were evaluated. The issues of compatibility between the filler packs and RTM resin processing conditions and the identification of manufacturing problems of each configuration were assessed.

Configuration Type	Filler Pack Type	Flange Cap Type
1	braided	3 plies of braided fabric
2	braided	none
3	adhesive	3 plies of braided fabric
4	adhesive	none

Table 21: Frame Flange Configurations for the 3 ft. Manufacturing Demonstration

### 3.E.2 Circumferential Hoop Frame Batch Mode Manufacturing

#### 3.E.2.a Tool Design

The RTM tool was designed to demonstrate the capability of RTM long thin structural components and the batch mode concept. Although the fabrication of the 3 ft. frames demonstrated simultaneous batch mode processing of two frames, the process is still valid for multiple frames. The tool contained a single resin injection port and distributed the resin uniformly around the frame cross section using a manifold. The mandrel and mold cavity were machined out of aluminium to accommodate both of the mouse hole configurations identified in global evaluation (Section 1.B.3) and local optimization (Section 4.C). Grooves were machined into the mandrel to place the braided preforms in tension to prevent fiber movement during injection; this groove was also used as a trimming aid. The dimensions of the tool cavity were determined through process manufacturing models and preform thickness measurements. The dimensions of the tool cavity were critical because they directly control the fiber volume fraction of the composite part.

#### 3.E.2.b Frame Preform Assembly

A schematic of the crown frame fabrication procedure is shown in Figure 14. As shown in the figure, the braiding mandrels are covered with six plies of triaxial braid. The ends of the preform were trimmed and then the braided mandrel was placed into the mold cavity. To prevent preform fraying, tackifier was applied to the individual plies along the cutting area. The top three plies were then cut along the length of the mandrel and folded to form the bottom "J" flanges. Once the radius filler packs were inserted, the flange cap was laid-up and the mold was closed. To fabricate a frame without a top cap, a brass shim plate was placed between the top cover and mandrel plies prior to RTM.

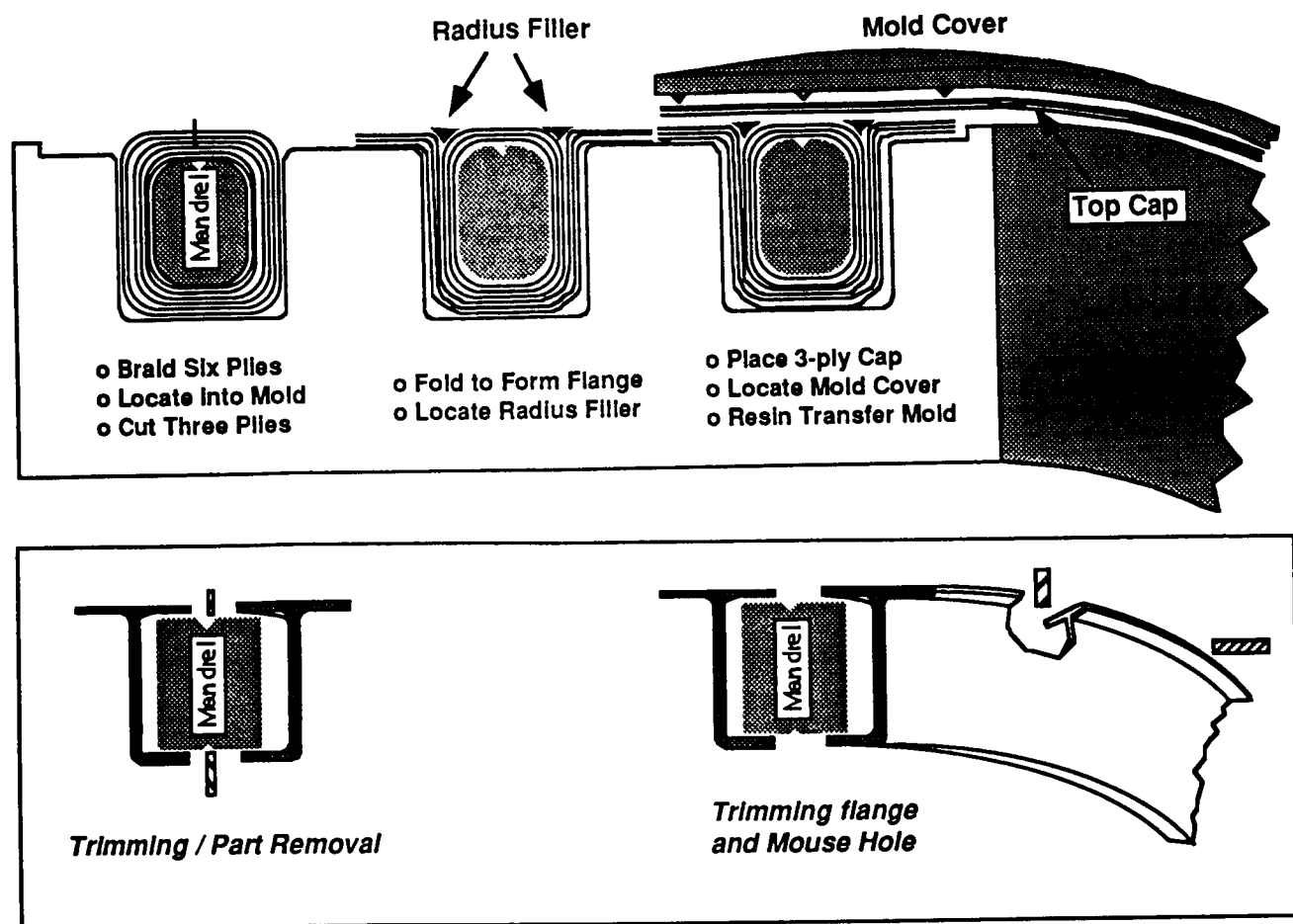


**Figure 14: Crown Frame Fabrication Procedure**

### 3.E.2.c RTM with Shell's 1895 Resin

The RTM mold was oriented in a vertical position during resin injection and curing. The lower injection port of the RTM tool was connected to the resin feed system and the upper port was connected to a vacuum system. The mold was checked for vacuum integrity and preheated to 250-280°F. The proper amounts of resin and hardener were measured, mixed, and degassed for approximately 10-20 minutes. The resin system was then preheated to 180-200°F.

The injection cycle started with the filling of the feed system. The mold was evacuated of all air and the resin was injected at 40-90 psi into the mold through the lower port. After the mold was filled, the vacuum was relieved and the mold was pressurized at 40-90 psi for the cure cycle. The cure cycle consisted of gel stages for 30 minutes at 300°F and for 90 minutes at 350°F. Following the gel stages, the mold was cooled to 250-275°F for part removal. A freestanding post cure of two hours at 350°F was the final step prior to trimming and finishing.

Frames manufactured early on in the manufacturing demonstration possessed some surface porosity. This porosity was eliminated by increasing the injection temperature to 235°F which lowered the injection viscosity of the resin. Another processing modification was the utilization of a carbon fiber veil which acted as a breather to evacuate entrapped air. The veil eliminated surface porosity and improved the frame surface finish.

A temperature controller maintained the desired tool temperatures throughout the RTM process. Thermocouples were located inside the mold cavity and braiding mandrel in order to monitor the temperature distribution and to prevent thermal gradients.

#### *3.E.2.d Part Removal and Trimming*

The part was trimmed off the mandrel with the aid of the cutting groove in the mandrel (Figure 14). After removal of the frames from the mandrel, the mouse holes and flange edges were trimmed as shown in Figure 15.

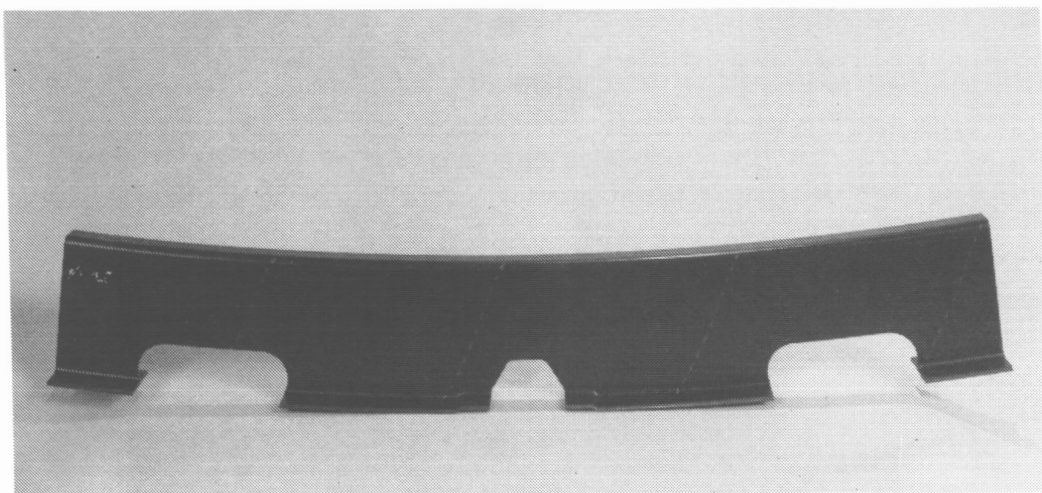


**Figure 15: Crown Panel Frame Following Trimming**

#### *3.E.2.e Quality Control Procedures*

The same quality control procedures described in Section 2.B.2 were used to evaluate the quality of the 3 ft. frames. Photomicrographs, resin digestion tests, and ultrasonic evaluations showed that the frames possessed void contents of less than 0.5%. Measurement of the nickel coated tracers yarns showed that the braid angles were within required tolerances. Finally, coordinate measurements showed that all frame dimensions were within specified tolerances.

## **4. LOCAL DESIGN OPTIMIZATION**

The circumferential frame design issues that were addressed in the local optimization phase of the ATCAS design process were: the flange cap configuration, the cap filler pack, the mouse hole configuration, and batch-mode tooling requirements. The overall objective of the local design optimization studies was to reduce the cost and weight of the frame configuration and address the technical issues identified in the global evaluation phase of design. The following sections summarize the past and present activities in the local optimization of the circumferential hoop frames.

### **A. Dimensional Accuracy Optimization**

The four frame designs described in Section 3.E.1 were used to identify the configuration that produced the optimum dimensional stability. The main concern was thermal warpage of the frames caused by material anisotropy and structural geometry. This concern was addressed by coordinate measurements of the 3 ft.

frame manufacturing demonstrations and finite element analysis. Key elements that directly affect the thermal warpage of the frames were: geometry, anisotropic architecture, the filler pack, the resin rich areas around radii bends that are inherent to the RTM process, and the flange cap. A combination of two key elements were varied in the finite element analysis: the type of filler pack and the flange cap configuration. The analysis used three-dimensional elements because of the different material properties across the frame cross-section (plane stress or plane strain conditions could not be applied to this particular problem).

All manufactured frames were found to experience flange spring-in and a small amount of web twist caused by the frame curvature in the hoop direction. A summary of frame coordinate measurements and finite element analysis results is shown in Table 22. The spring-in of the frames varied from 0.3° to 0.6°. Configuration Type 3 experienced the least amount of spring-in because the combination of the adhesive filler pack and braided cap offer the most resistance to flange deformation. Configuration Type 2 experienced the most spring-in because to the braided filler pack offered little resistance to flange deformation. The dimensional stability finite element analysis successfully predicted the configuration that minimized the spring-in deflection; predicted values were within 10% of all measured values. It is noted that the finite element analysis did not predict web twist because the frame curvature in the hoop direction has not yet been incorporated.

Configuration Type	Measured Flange Spring-In (degrees)	FEM Predicted Flange Spring-In (degrees)	Measured Web Twist (degrees)
1	0.3	0.28	0.025
2	0.6	0.56	0.025
3	0.3	0.27	0.065
4	0.6	0.54	0.065

**Table 22: Correlation Between Measured and Predicted Flange Spring-In**

Although the configuration consisting of the adhesive filler pack and braided cap minimizes flange spring-in, the spring-in deflections of all types of configurations are within reasonable limits (under 1°). Therefore, it was concluded that any of the four frame design configurations (with the proper tooling) would hold the necessary frame tolerances.

## **B. Frame-to-Skin Bond Issue**

Two university subcontracts are supporting ATCAS efforts on the technical issues of frame-to-skin bond strength and durability. The University of Washington is characterizing viscoelastic properties of the adhesive. To date, time and temperature dependent properties for dry samples have been measured. Drexel University is performing three tasks: 1) time-dependent analysis development, 2) fracture toughness test characterization, and 3) frame-to-skin adhesive bond element tests. To date, significant progress has been achieved in the first two tasks. Adhesive fracture tests have been performed with braided composite plate adherends of the same architecture as the final crown frame design. Results indicate relatively high bond line fracture toughness, despite the tendency for cracks to propagate outside the toughened adhesive layer. A "rough" fracture surface that replicates the braided plate architecture appears to be responsible for the high toughness.

As a result of the test data, Type 4 was chosen as the locally optimized configuration. The skin attachment flange for frame elements of the locally optimized crown design have a thickness equal to half that of the frame web and top flange. In the original design, an additional braided plate was included as part of the frame flange that attached to the skin, resulting in a thickness equal to that of the web and similar thickness to the skin. This additional plate was included in the design as a manufacturing aid; however

subsequent process trials indicated that it was not needed. The reduced thickness of the current frame flange that is bonded to the skin is not only expected to reduce cost and weight, but also improve bond strength.

### C. Mouse Hole Configuration

Manufacturing costs and risks were evaluated via comparative studies for several mouse hole configurations during the local optimization process. As a result of the comparative studies, several design modifications were identified to reduce manufacturing costs and to simplify the frame/stringer/skin assembly. The most significant design modification was a larger frame mouse hole with a simplified configuration; this design modification is shown in Figure 16. The optimized configuration reduced tolerance build-up at the frame/stringer/skin interfaces, assembly time, and the manufacturing cost of the

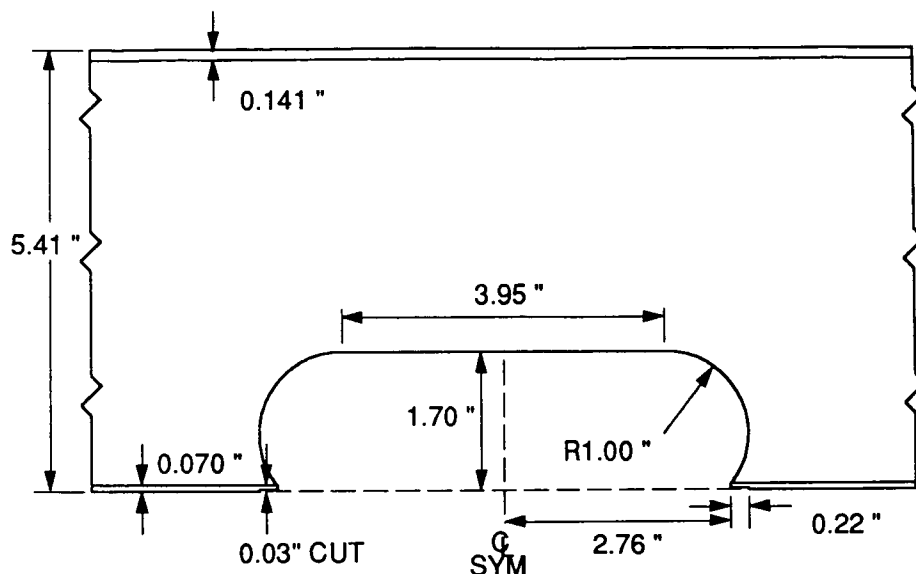


Figure 16: Mouse Hole Configuration Following Local Optimization

In the optimized configuration, the frame is not directly bonded to the stringer, which minimizes the difficulty of bonding three elements (frame/stringer/skin) at one intersection. Assembly costs were reduced by 0.6% and the frame weight was reduced by 8.5% by eliminating the need for a rotisserie assembly tool. The original assembly method restricted the ability to place frames on a preassembled skin-stringer panel; the new mouse hole configuration eliminated this restriction. The DBT determined that the modification to a larger mouse hole would require further testing to evaluate the impact upon structural performance. The structural performance of the original mouse hole design (Figure 5) and the optimized configuration will be evaluated via large scale testing of the crown panel.

### D. Manufacturing Process Optimization

Batch-mode tooling requirement modifications were responsible for significant cost savings. Factory simulation studies showed that sixteen RTM tools could be reduced to five and still meet the desired crown panel production rate. This modification resulted in a 16.2% reduction in frame cost [10].

Another modification in the manufacturing process optimization was the tapering of the frame flanges. This modification was made to increase the pull-off strength of the frame-to-skin bond and to reduce the risk of manufacturing problems; this modification did not have a significant impact on frame cost or weight. Tapering the flanges minimized resin pools and reduced the stress concentrations at the edges of the flanges. It also reduced the probability of tooling interferences and cure bagging risks [10].

### E. Cost and Weight Impact of Local Design Optimization

The changes made to the circumferential hoop frame design during the local optimization phase showed cost savings of 30.1% and weight savings of 13.3% over the original frame design selected in the global evaluation phase. These modifications reduced the overall crown panel cost by 3.2% and overall weight by 2.8% as indicated in Table 23. Although some of the frame design and manufacturing modifications did not project costs or weight savings, they were incorporated to improve the overall manufacturing process and to reduce the risk of anomalies.

Global Evaluation	Local Optimization	Purpose of Change	Optimization Method	Cost Savings	Manufacturing Risk	Structural Performance
Small Mouse Hole	Wider Mouse Hole	- Reduce tolerance build-up - Reduce tooling cost	- DBT - Demonstration	0.6 %	Reduced	TBD
16 tools	5 tools	- Reduce tooling cost	- Factory Simulation	16.2 %	NA	NA
3 Plies of Braided Fabric	No Cap	- Increase performance - Reduce cost - Reduce weight	- DBT - Demonstration	13.3 %	Reduced	Increased
Several Potential Configurations	Adhesive Filler Pack	- Increase damage tolerance	- Design Analysis - Demonstration	0 %	Reduced	Increased
Flange Edge	Tapered Edge	- Minimize resin pools - Lower cure bagging risks - Increase pull-off strength	- Structural Tests - Demonstration	0%	Reduced	Increased

Total Frame Cost Savings	30.1 %
Total Frame Weight Savings	13.3 %
Total Crown Panel Cost Savings	3.2 %
Total Crown Panel Weight Savings	2.8 %

**Table 23: Summary of Locally Optimized Frame Cost and Weight Savings**

### F. Summary of Current Circumferential Hoop Frame Design

The current circumferential hoop frame configuration developed by the global evaluation and local optimization studies is shown in Figure 17. This is the configuration that will be manufactured during the scale-up 8 ft. frame manufacturing demonstration at the end of 1991.

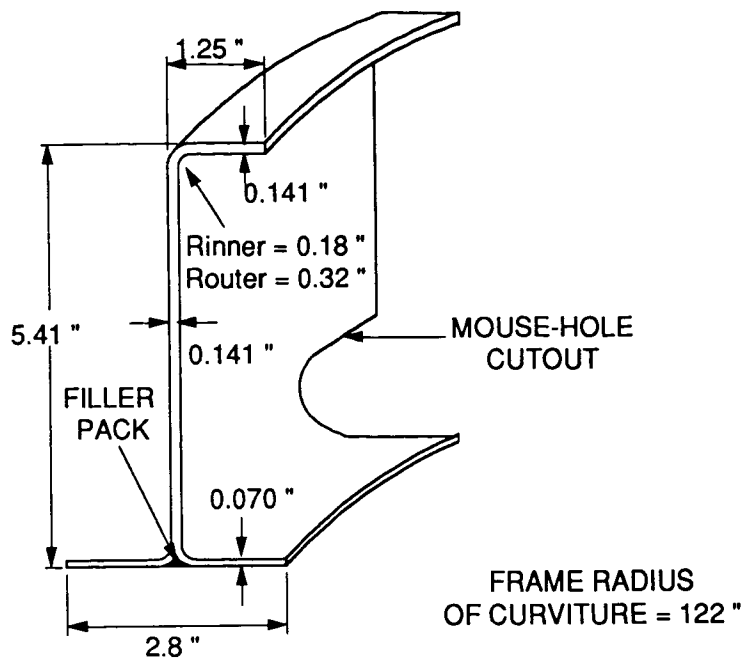


**Figure 17: Circumferential Hoop Frame Configuration Following Local Optimization**

## FUTURE WORK

### Approach to Scale-up

The manufacturing demonstration of the 3 ft. frames provided processing information essential for the production of full-size 16 ft. long crown frames. The processing conditions for the Shell 1895 resin system met the manufacturing criteria, but additional work must be performed to fully understand the resin processing window and associated structural performance with triaxially braided preforms. The 3 ft. frame demonstration demonstrated the feasibility of batch mode processing with net-shape braided preforms. The frame flange spring-in, web twist, and dimensions were controlled by process optimization and tooling accuracy ( $\pm 0.010$  inch tolerance on all frame dimensions). Tooling design for longer frames must be supported by additional trials and FEM models to ensure that the frame dimensions are held to  $\pm 0.010$  inches. Although the 3 ft. frames were not fabricated with a fully automated braiding and RTM systems, the demonstration proved the manufacturing proof of concept and requirements, and provided insight for risk and cost reduction for scale-up activities.

### 8 ft. Frame Manufacturing Demonstration

The fabrication methods that were addressed during the manufacturing demonstration of the 3 ft. frames will be utilized to develop the manufacturing process for 8 ft. frames. The RTM tool will be fabricated with Invar 36 material to minimize thermal warpage caused by tool-to-part CTE mismatch and maximize dimensional accuracy. The 3 ft. tool design will be modified to accommodate the design modifications made during the local optimization phase of the ATCAS design process. The tool will accommodate the thinner bottom frame flange and the flange spring-in effects. The stringer flange joggle that was needed for the original mouse hole configuration will be eliminated so that the tool may be used for any stringer spacing. The RTM processing parameters used to fabricate the 3 ft. frames will be used as the baseline. Additional process optimization for improved part quality will be conducted during the 8 ft. frame fabrication demonstration. The temperature control techniques that will be used to manufacture the 8 ft. frames will be similar to the techniques used in the 3 ft. manufacturing demonstration.

More than fifteen 8 ft. frames will be produced and evaluated during the last quarter of 1991. Evaluations will include: warpage measurements at  $-30^{\circ}\text{F}$ ,  $75^{\circ}\text{F}$ , and  $130^{\circ}\text{F}$ , void content, resin distribution, fiber orientation, and dimensional accuracy. Following inspection, the frames will be co-bonded onto three 7 ft by 10 ft. skin-stringer assemblies (Figure 18). The integrity of the entire crown panel structure will be evaluated by large panel tests.

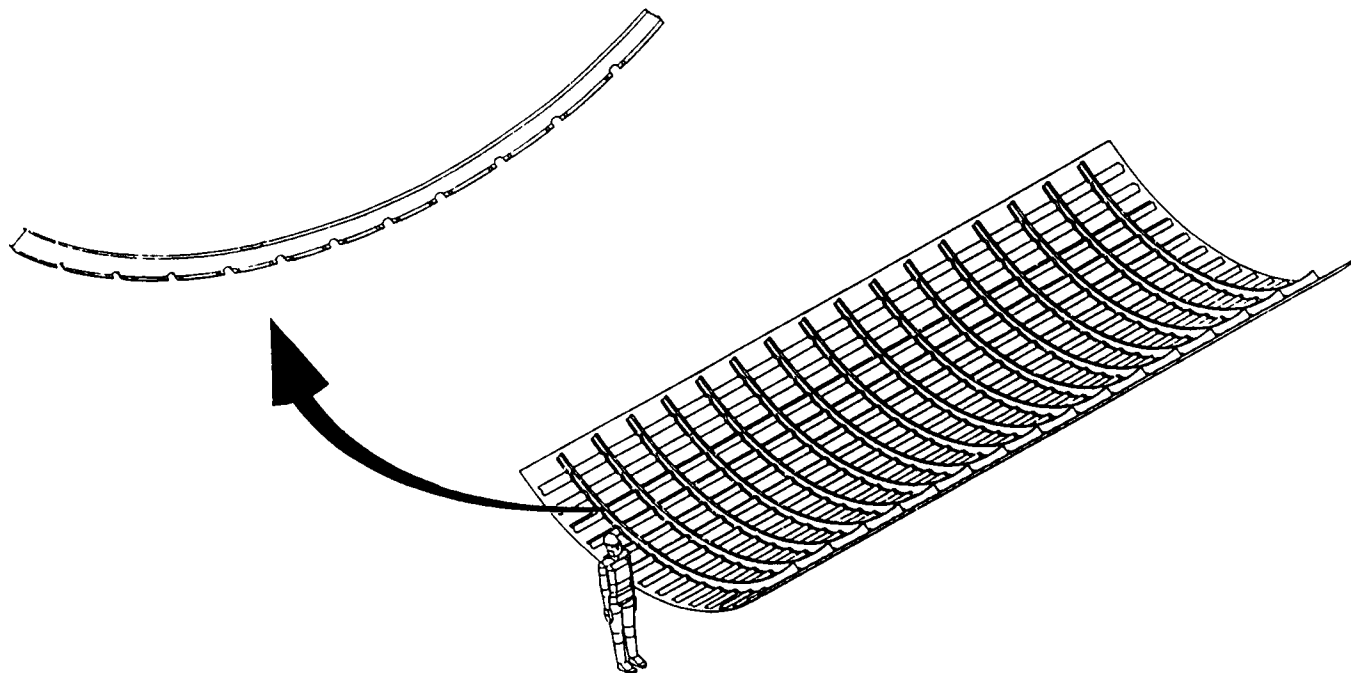


**Figure 18: Crown Panel Assembly**

### **Verification Cost and Test**

Detailed cost and weight studies will be performed during the 8ft. frame manufacturing demonstration. The costs and weight associated with the 8 ft. frames will be utilized in the final crown panel cost and weight studies. Although the costs studies based on automation will not provide a final answer, the manufacturing and process modifications needed to meet production criteria will be determined.

## **KEY ACCOMPLISHMENTS**

The ATCAS Team has shown that textile composites can successfully be applied to primary fuselage structural components. The crown circumferential frames (Figure 19) were designed, characterized, and manufactured through the efforts summarized in this paper. The ATCAS three step design process and the DBT approach were successfully demonstrated. The state-of-the-art in textile technology was advanced in the areas of design, materials, manufacturing, analysis, and test. The technology developed in this effort was successfully applied to a direct application. The low cost manufacturing approach selected for the crown frames was demonstrated via a 3 ft. manufacturing demonstration. Finally, the scale-up issues that need to be addressed for the 8 ft. frame manufacturing demonstration were identified and are currently being analyzed.

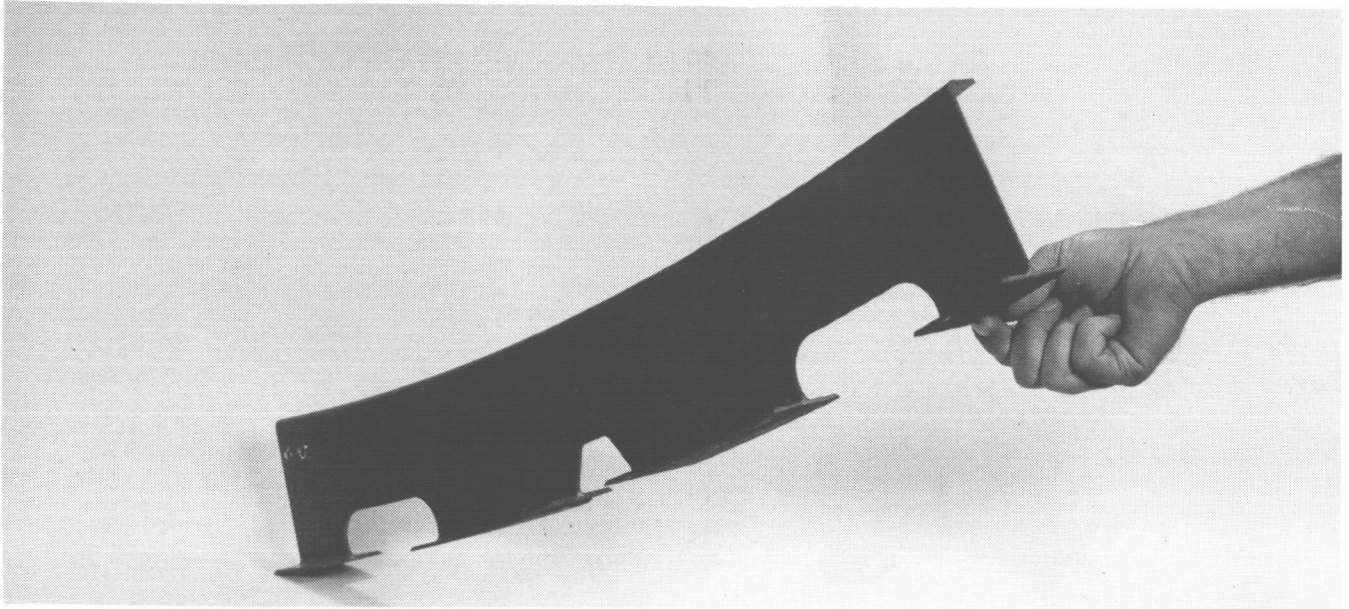


**Figure 19: Crown Panel Frame Fabricated During Manufacturing Demonstration.**

## **ACKNOWLEDGMENTS**

The authors would like to gratefully acknowledge the efforts of the following Boeing personnel who contributed to this effort: Dr. Christian Gunther, Dr. Pierre Minguet, Dr. Larry Ilcewicz, Adam Sawicki, and Blake Flinn. The authors would also like to thank the following subcontractors and organizations for their efforts and cooperation throughout the ATCAS Program: 1) Garrett Sharpless and Steve Goodwin at Fiber Innovations Inc., 2) Ralph Hewitt, Dr. Eric Stark, and Diane Henry at Shell Chemical Co., and 3) Dr. Charlie Harris, Buddy Poe, and John Masters at the Mechanics of Materials Branch at the NASA Langley Research Center.

## REFERENCES

- 1 Walker, T.H., Smith, P., Truselove, G., Willden, K., Metschan, S., Pfahl, C., " Cost Studies for Commercial Fuselage Crown Designs", First NASA Advanced Composite Technology Conference Proceedings, Seattle, WA, October 29-November 1, 1990, NASA-CP-3104.
- 2 L.B. Ilcewicz, P. Smith, T.H. Walker, R. Johnson, " Advanced Technology Composite Aircraft Structures", First NASA Advanced Composite Technology Conference, Seattle, WA, October 29-November 1, 1990, NASA-CP-3104.
- 3 Nui, M.C., *Airframe Structural Design*, Conmilit Ltd., 1988.
- 4 Fedro, M.F., Gunther, C.K., Ko, F.K., "Mechanical and Analytical Screening of Braided Composites for Transport Fuselage Applications", *First NASA Advanced Composite Technology Conference Proceedings*, Seattle, Washington. October 29 - November 1, 1990. pp. 677 - 704.
- 5 ASTM Standards and Literature References for Composite Materials, First Edition, Editor R.A. Storer, ASTM Philadelphia, Pa., 1987.
- 6 Gause, L.W., Alper, J.M., "Structural Properties of Braided Graphite/Epoxy Composites", *Journal of Composites Technology & Research*, Vol. 9, No. 4, Winter 1987, pp. 141-150.
- 7 Whyte, D.W.: On the Structure and Properties of 3-D Braided Reinforced Composites. PhD Thesis, Drexel University, June 1986.
- 8 Adams, D.F., Walrath, D.E., "Iosipescu Shear Properties of SMC Composite Materials," *Composite Materials: Testing and Design (Sixth Conference)*. ASTM STP 787, American Society for Testing and Materials, 1982, pp 19-33.
- 9 Martin, R. "Delamination Failure in a Unidirectional Curved Composite Laminate", *NASA Contractor Report 182018*, Contract NAS1-18599, April 1990.
- 10 K.S. Willden, S. Metschan, "Composite Fuselage Crown Panel Manufacturing Technology", Ninth DoD/NASA/FAA Conference on Fibrous Composites in Structural Design, NASA CP ,19 .(Paper of this compilation).